# GBIR CROSSTALK REDUCTION OF FULLY POLARIMETRIC DATA FROM BLUE SPRINGS DAM

---

A Thesis

presented to

the Faculty of the Graduate School

at the University of Missouri-Columbia

---

In Partial Fulfillment

of the Requirements for the Degree

Master of Science

by

SATYA SRINIVASU CHERUKUMILLI

Dr. Justin Legarsky, Thesis Supervisor

July 2012

# APPROVAL PAGE

The undersigned, appointed by the dean of the Graduate School, have examined the thesis entitled

GBIR CROSSTALK REDUCTION OF FULLY POLARIMETRIC DATA FROM BLUE SPRINGS DAM

presented by Satya Srinivasu Cherukumilli,

a candidate for the degree of master of science,

and hereby certify that, in their opinion, it is worthy of acceptance.

_____

Dr. Justin Legarsky

_____

Dr. Brent Rosenblad

_____

Dr. Zhihai (Henry) He

# ACKNOWLEDGEMENTS

I owe my deepest gratitude to my academic advisor, Dr. Justin Legarsky, who had faith in me and made his support available to me in a number of ways without which this could have never been possible. I would also like to thank my radar team members and mentors, Dr.Francisco (Paco) Gomez and Brent Rosenblad for their support.

Lastly, I would like to offer my regards to all of those who supported me in any respect during this project.

Satya Cherukumilli

# Table of Contents

# LIST OF FIGURE

# LIST OF TABLES

# ABSTRACT

An investigation into reducing crosstalk from Blue Springs Dam GBIR fully polarimetric data was conducted. Advanced polarimetric processing and techniques often rely on precise phase measurement. One benefit of crosstalk reduction is improvement in phase measurement. A well-known model of crosstalk behavior was explored in relation to the MU GBIR. To achieve a successful estimation of the method parameters, data culling was performed to weed out low cross-polarization and high-correlation values from the processing flow. After data culling, average covariance matrices were formed for use in crosstalk parameter estimation. Analysis of crosstalk parameters demonstrated the values had small fluctuation over the unmasked locations. Using global estimates, calibration correction matrices were formed and applied to the data. The resulting crosstalk calibrated imagery showed a reduction in crosstalk of about 9 dB. Thus, the Blue Springs Dam polarimetric data were successful crosstalk calibrated.

# CHAPTER 1. INTRODUCTION

## 1.1 Satellite-Based Interferometric RADAR

Satellite-based interferometric RADAR may be used measure topography and various surface movements. Although satellite-based measurements have a number of important uses and applications, current commercial satellite RADAR may have limitations in a number of scenarios. These limitations may arise due to a number of issues such as temporal resolution, spatial resolution, RADAR frequency, polarization, and atmospheric effects [Werner *et al.*, 2009]. A number of these limitations may be overcome by an in situ radar imaging system [GAMMA, 2011].

## 1.2 MU Ground Based Interferometric Radar

Limitations in the current commercial satellite-based SAR datasets are being addressed in part by a specialized (dual-frequency, polarimetric, and interferometric) ground-based real-aperture RADAR (GBIR) instrument developed by the University of Missouri (MU) team in partnership with GAMMA Remote Sensing. The high temporal resolution is well suited for measurements of rapid deformation. The highly portable GBIR may be deployed to obtain data with high spatial resolution (i.e. on the order of 1 meter) and high temporal resolution (i.e. on the order 1 minute). From the equivalent geodetic position, the GBIR may collect dual frequency data set using C-band and Ku-band. In addition to interferometry, vector scattering may be investigated using the GBIR fully polarimetric capability at C-band operation.

The MU GBIR system has been deployed in a number of field sites. A number of United States Army Corps of Engineers (USACE) dams in Missouri and Kansas have been imaged using the GBIR sensor. Also, a number of landfills in Colorado and Missouri have been imaged. Millimeter scale sensitivity has been demonstrated using the MU GBIR.

Precision phase measurements are important in advanced radar processing such as interferometry and polarimetry. Crosstalk may degrade the signal phase integrity (i.e. lower performance). Thus, crosstalk reduction of GBIR is desired.

### 1.3 Thesis Overview and Organization

This thesis details an investigation of crosstalk reduction of Blue Springs Dam and vicinity fully polarimetric GBIR data. During the study, a number of processing steps were conducted and investigated. For GBIR crosstalk calibration, a well known model [Quegan, 1994] was applied. For estimating global model parameters the data were culled for high correlation and low cross polarization power. Crosstalk calibrated images of Blue Springs site are generated and discussed.

Thesis organization includes an introduction in Chapter 1, RADAR fundamentals in Chapter 2, GBIR polarimetric methodologies in Chapter 3, Blue Springs Dam site overview in Chapter 4, a presentation of the results and discussion in Chapter 5, a concluding discussion and future work direction in Chapter 6, and listings of the thesis references in Chapter 7.

# CHAPTER 2: RADAR FUNDAMENTALS

RADAR and RADAR methodologies are covered thoroughly in the open literature. Two major advantages of microwave RADAR imaging over visible optical imaging are imaging capabilities through weather (e.g. clouds) and day/night imaging capability [Richards, 2005]. This chapter provides a brief overview of the relevant methods and theory utilized in this investigation.

## 2.1 Fundamentals of RADAR

### *2.1a. Simple Pulse RADAR*

RADAR systems may perform a number of functions such as detection, range tracking and scene imaging. The two-way travel time, $\tau_{2\text{-}way}$, required for an electromagnetic (EM) simple pulse to propagate a distant $R$ and return is given by

$$\tau_{2-way} = \frac{2R}{v} \tag{2.1}$$

where $v$ is the speed of light. Figure 2.1 illustrates an example block diagram for a simple-pulse monostatic RADAR system [Richards, 2005].

A monostatic RADAR uses collocated antennas (e.g. same antenna) both transmission and reception of the EM wave. In the example from Figure 2.1, a waveform generator outputs a desired pulse to the transmitter, which shifts the waveform to the desired radio frequency and amplifies the signal its power level specification before feeding the signal to the antenna for EM wave transmission. After transmission, the EM

wave propagates through the media and interacts with targets encountered. The interactions may result in a scattering of the EM wave of sufficient level back toward the receiver, which collects this into a return signal. In the example, the return signal is conditioned and amplified by a low-noise RF amplifier before being shifted to an intermediate frequency for signal processing, data processing, and display.

For a pulse RADAR, the interval between two successive transmitted pulses is called the pulse repetition interval (PRI) and its inverse is called pulse repetition frequency (PRF) [Skolnik, 2008]. The range resolution cell is the volume in space that contributes to the echo received by radar at instant given time interval. Figure 2.2 illustrates the resolution in range dimension for a simple pulse RADAR.

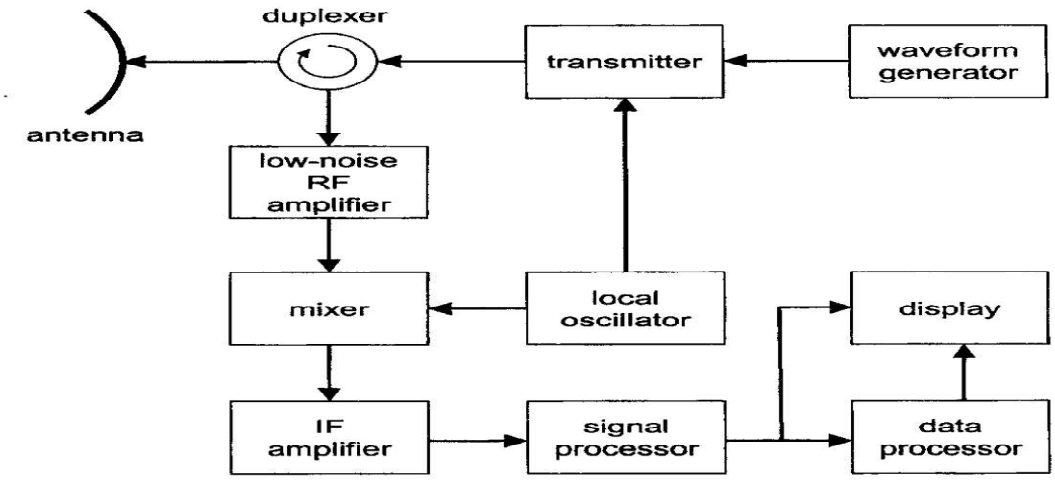


**Figure 2.1**. Block diagram illustrates an example configuration of a simple-pulse monostatic RADAR System [Richards, 2005].

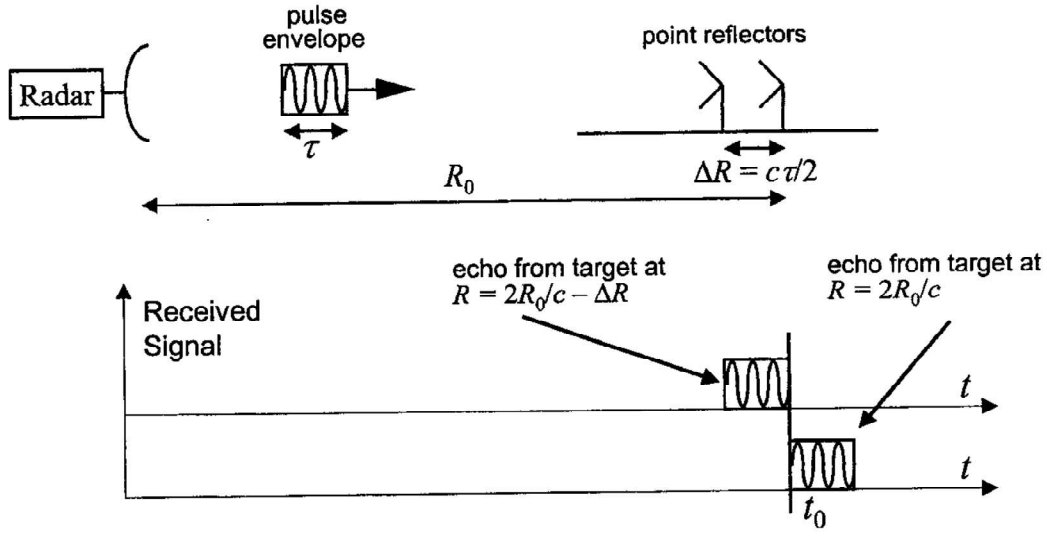


**Figure 2.2.** Diagram illustrates target resolution in time and range for as simple pulse RADAR. Here, the range resolving ability to distinguish between two targets may found as half the product of the speed of light with the simple pulse duration [Richards, 2005].

*2.1b. Linear up-chirp FM RADAR*

Linear frequency modulation (FM) modulated continuous wave radar allows decoupling of range resolution and modulation waveform duration. For each up chirp duration (i.e. the modulation rate, $f_m$, is one over the duration), the frequency is linearly swept over the waveform bandwidth, $B$, from the minimum frequency to the maximum frequency as shown in Figure 2.3. As return signal arrive, the returns and the reference may be combined to produce a beat frequency, $f_b$, proportional to range (i.e. the ratio of $B$ to inverse $fm$ equals the ratio of $f_b$ to $2R/v$) [Tamatsu *et. al*, 1997] as

$$f_b = \frac{2BRf_m}{v} \quad . \tag{2.2}$$

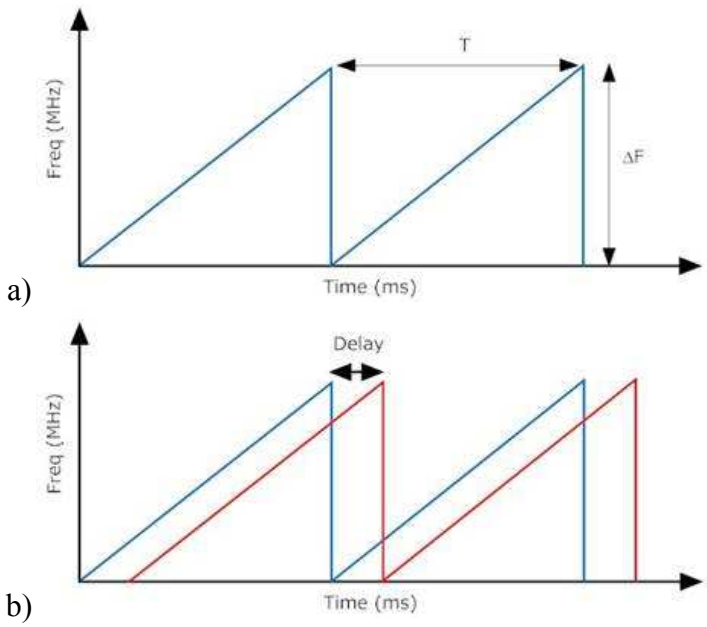


**Figure 2.3.** Plots illustrate the linear FM up chirp concept. a) A reference chirp frequency versus time is shown. b) Return chirp (red) and reference chirp (blue) frequencies are shown as functions of time [Advsolned].

A Fourier transform of the time domain beat frequency signal represents the return signal as a function of time (i.e. time proportional to the target range as equation 2.1) [Tamatsu *et al*., 1997]. The range resolution is determined by the wave's velocity of propagation, *v*, (i.e. speed of light) and the waveform bandwidth, *B*, [Elachi and Zyl, 2006] given as

$$r_R = \frac{v}{2B} = \frac{v\tau_{eff}}{2} \tag{2.2}$$

$$\tau_{eff} = \frac{1}{B} \tag{2.3}$$

where $\tau_{eff}$ is the effective pulse duration after processing the return signal [Richards, 2005] as shown in Figure 2.4.

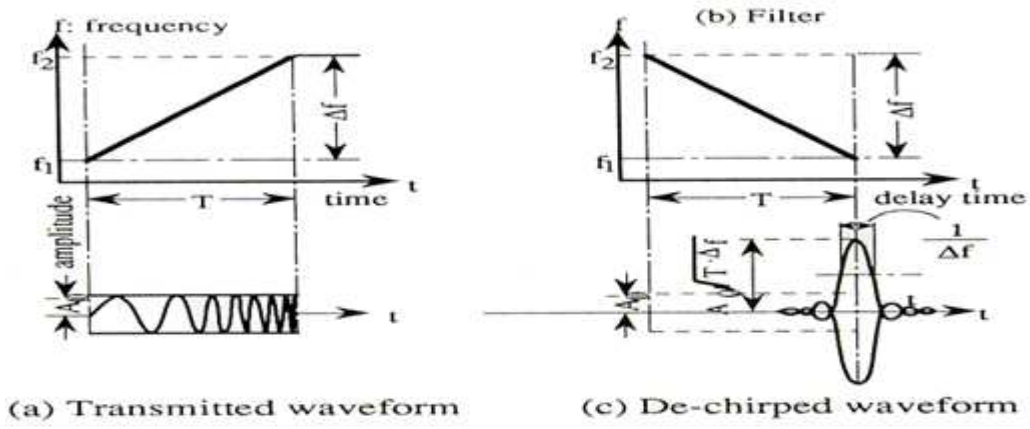


**Figure 2.4**. Effective pulse length for a linear frequency modulated signal. a). Transmitted waveform is shown. b) Effective pulse waveform is shown after processing [Radar Tutorial].

*2.1c. Received Signal Overview*

The RADAR transmitted EM wave expands outwardly in the form of spherical waves. Far away from the RADAR, the spherical EM wave front appears nearly planar [Ulaby, 2007]. This far-field region may be defined for the ranges as [Richards, 2005],

$$R_{\text{far field}} \geq \frac{2D^2}{\lambda} \tag{2.4}$$

where D refers to the antenna maximum dimension and $\lambda$ is the EM wavelength. A transverse EM plane wave's vector amplitude may be written as [van Zyl and Kim, 2011]

$$\vec{A} = a_h e^{j\delta_h}\hat{h} + a_v e^{j\delta_v}\hat{v} \tag{2.5}$$

where $\hat{h}$ and $\hat{v}$ are the orthogonal (e.g. horizontal and vertical) unit vectors, $a_h$ and $a_v$ are real valued amplitudes, and $\delta_h$ and $\delta_v$ are the real valued relative phases. Polarization refers to the shape traced out by the tip of the electric field over time at a fixed point in space [van Zyl and Kim, 2011].

A radiation pattern describes the directional characteristic of an antenna. A common pattern for imaging radar use a single main lobe surrounded by minor lobes. The main lobe may be summarily characterized by calculating its orthogonal half-power beam widths (one in azimuth $\beta_{az}$ and the other in elevation $\beta_{el}$) and its maximum gain, $G$. The minor lobes response may be summarized by the ratio of the maximum minor lobe to the main lobe maximum. For dual fed orthogonally polarized antennas, the crosstalk from one feed to the other may summarize the polarization purity of the antenna.

For received power consideration, a target's scattering behavior may be described by the RADAR cross section (RCS), $\sigma$, which is an area quantity. If the power collected by an RCS area is reradiated isotropically (i.e. radiates the same in all directions), then the same scattered power density will produced as by the actual target [Richards, 2005]. The monostatic radar range equation [Ulaby *et al*., 1982] for a target may be written as

$$P_r = \frac{P_t G^2 \lambda^2 \sigma}{(4\pi)^3 R^4} \tag{2.6}$$

To calculate the average power over space and time for many targets, the differential scattering coefficient (i.e. sigma nought) is defined as the average value of the scattering cross-section per unit area [Ulaby *et al*., 1982], written as

$$\sigma^0 = \langle \frac{\sigma_i}{\Delta A_i} \rangle \tag{2.7}$$

where $\sigma_i$ is the radar cross section of target $i$, $\Delta A_i$ is the area associated with $\sigma_i$, and <> is the average operation. Assuming an effective pulse-limited scenario and unchanging parameters and range over the illuminated area, the radar cross section [Richards, 2005] may be written approximately as

$$\sigma = \sigma^0 A_{ill} \tag{2.8}$$

where $A_{ill}$ is the illuminated area. $A_{ill}$ may be approximated for a flat surface with small azimuth angle (e.g. as shown in Figure 2.5) [Richards, 2005] as

$$r_g = \frac{r_R}{sin\theta_{inc}} \text{ for flat surface} \tag{2.9}$$

$$r_{az} = 2Rsin\left(\frac{\beta_{az}}{2}\right) \approx R\beta_{az} \text{ for small angles and flat surface} \tag{2.10}$$

$$A_{ill} = r_g r_{az} = \frac{r_R}{sin\theta_{inc}} R\beta_{az} \tag{2.11}$$

where $r_g$ is the ground range resolution, $r_{az}$ is the azimuth resolution, $r_R$ is the slant range resolution, $\theta_{inc}$ is the associated look angle of incidence, $R$ is the associated range, and $\beta_{az}$ is the azimuth half-power beam width in units of radians. With the given assumptions, the monostatic pulse-limited area scatterers form of the radar range equation [Skolnik, 1990] may be written as

$$P_r = \frac{P_t G^2 \lambda^2 \sigma^0 A_{ill}}{(4\pi)^3 R^4} = \frac{P_t G^2 \lambda^2 \sigma^0 r_R \beta_{az}}{(4\pi)^3 R^3 sin\theta_{inc}} \quad . \tag{2.12}$$

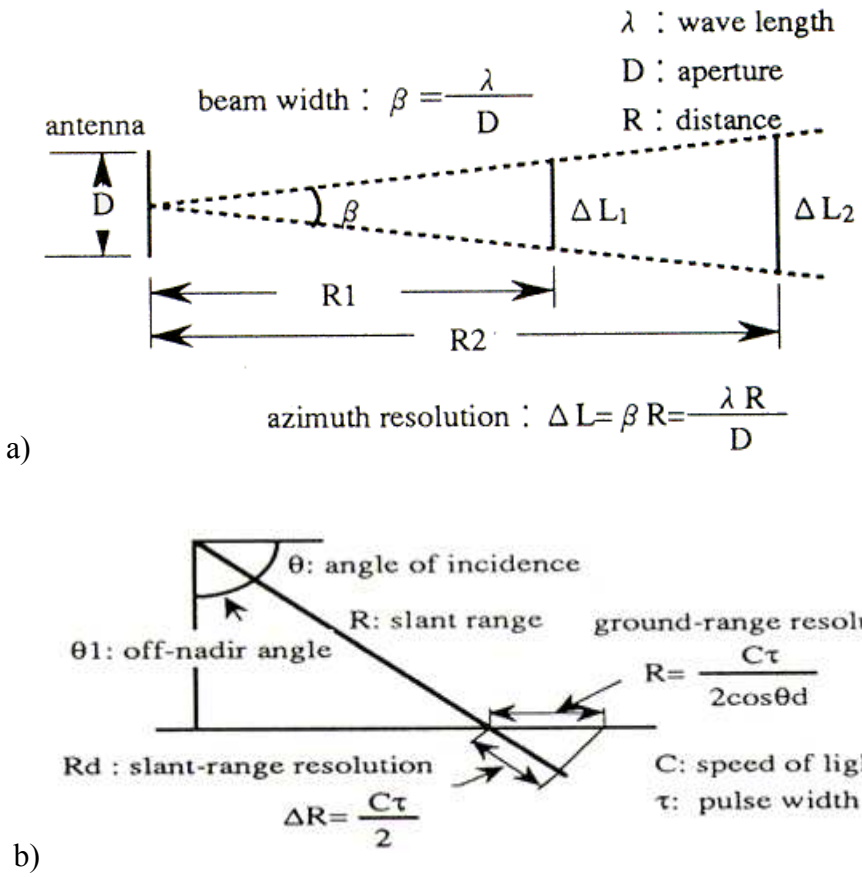


**Figure 2.5**. Diagrams illustrate pulse-limited RADAR and resolution. a) Azimuth resolution is illustrated. b) Slant range and ground range resolutions are illustrated [Radar Tutorial].

## 2.2 RADAR Imaging Overview

RADAR imaging may be accomplished by moving or scanning an antenna over a scene of interest as shown in Figure 2.6. Here, real-aperture RADAR (RAR) imaging is considered. For an antenna rotating horizontally about a fixed point, the signals may be transmitted and received as a function of the horizontal scan angle. The following overview considers a flat surface (i.e. topography may be considered for non-flat surfaces). From each effective pulse, a return signal in azimuth may be sampled. As the

RAR imager scans in azimuth, $N$ azimuth lines may stored. For each azimuth line, typically $M$ range bin samples are collected. The total angle scanned is $\theta_{scan}$ in degrees at the scan rate, $\Delta\theta$, in degrees per azimuth line. Consequently, an $N$ x $M$ sized image may be formed in polar coordinates (e.g. N rows cover the azimuth angles. M columns cover the RADAR slant range). Polar to rectangular coordinate conversion may be applied to aid visualization in rectangular coordinate system. If the RAR collects more than 1 return signal per effective pulse, then decimation may be applied (i.e. anti-alias low pass filter followed by down sampling [Oppenheim and Schafer, 1989]). Decimation provides a signal-to-noise ratio improvement of approximately the decimation factor. A short overview of decimation follows.

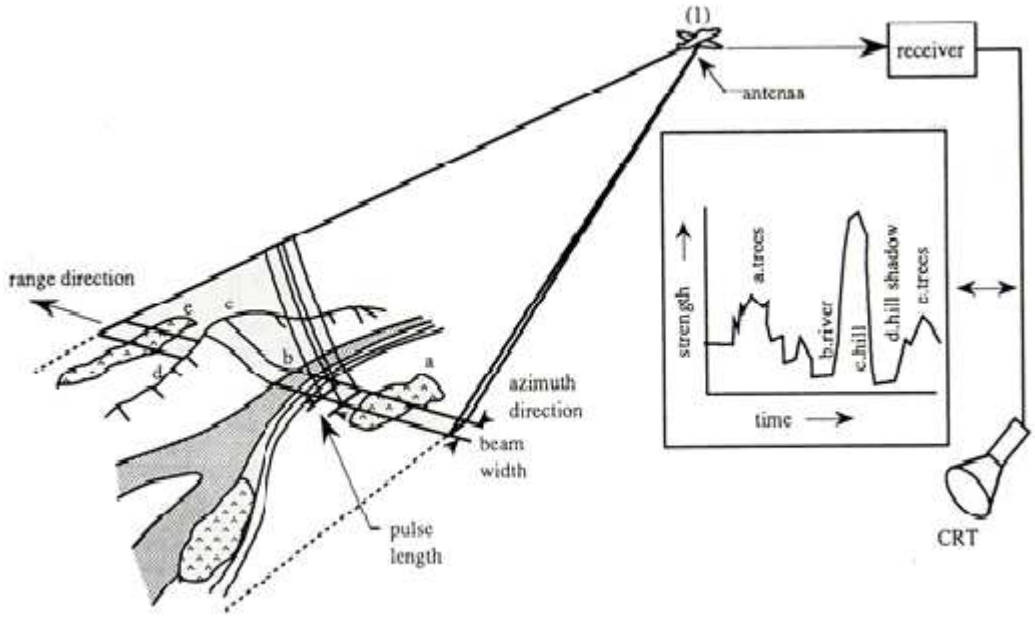


**Figure 2.6**. Illustration of a scene imaged by an effective pulse RADAR is shown. [Radar Tutorial].

A decimation factor, $D$, based on minimum fraction of overlap, $K$, may be formed as follows:

$$D = \text{floor}\left\{\frac{N}{\theta_{scan}}\beta_{az}(1-K)\right\} = \text{floor}\left\{\frac{1}{\Delta\theta}\beta_{az}(1-K)\right\} \quad (2.13)$$

where floor is the mathematical operation of rounding down to the nearest integer. After decimation, there are $M$ azimuth lines remaining given as

$$M = \text{floor}\left\{\frac{N}{D}\right\} = \text{floor}\left\{\frac{N\,\Delta\theta}{\beta_{az}(1-K)}\right\} \quad (2.14)$$

with an effective decimated scan rate given by

$$\Delta\theta_M = D\,\Delta\theta \quad (2.15)$$

For example, given K = 0.8 or 80% overlap for a 0.5° azimuth beam width would result in a decimated scan rate of about 0.1° (i.e. $\beta_{az}$(1-$K$)) since the floor function truncates the decimal point it may be slightly less than 0.1° as by equation 2.15.

**2.3 GBIR**

An MU team in conjunction with GAMMA Remote Sensing developed a specialized (dual-frequency, polarimetric, and interferometric) ground-based real-aperture RADAR (GBIR) instrument. A summary of the GBIR is presented here (see Tables 2-1, 2-2, and 2-3 for specifications summary) further details may be found in the user manual [GAMMA, 2011].

MU GBIR instrument uses real-aperture imaging. Three antennas may be mounted parallel to one another on a 1 meter high tower that may be precisely rotated. In the

interferometric mode and single polarization mode, there is one antenna used to transmit and two receiving antennas. In fully polarimetric mode, one antenna transmits H polarization followed by V polarization repetitive sequence and one antenna receives both H and V returns. Figure 2.7 illustrates and summarizes the various outer components of the MU GBIR.

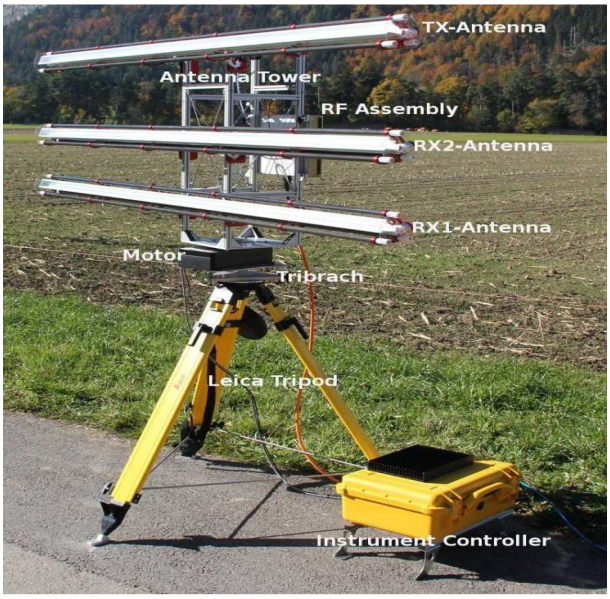


**Figure 2.7**. An example setup of MU GBIR's external components is shown. [GAMMA, 2011].

The GBIR primary subsystems are summarized as 3 Antennas per band (e.g. 1 transmit, 2 receive), 1 RF Assembly Box per band, 1 Instrument Computer; 1 Antenna tower with attached GPS antenna, 1 Leica tripod with 3 aluminum rods, 1 Instrument Cord, Power Cord, 1 Positioner with tribach leveler, and 1 Laser Plummet Battery Pack. The scanner on GBIR uses a stepper motor device that has a repeatability of 5 arc-sec, and a resolution of 0.36 arc-seconds (e.g. The approximate rotational scan velocity is in the range of 5-10 degrees/second) [GAMMA, 2011; Werner *et. al*, 2009].

For the fully polarimetric mode, Rx2 may attach to V Port (vertical) – upper, Rx1 may attach to H Port (horizontal) – lower, and TX H/V may attach to H/V Ports of the top antenna – above (i.e. Figure 2.8). Under this configuration, 4 single-look complex (slc) files may be generated [GAMMA, 2011] with the naming convention that follows:

1. Run once with gpri2_proc.py in -t TX_ANTENNA mode to V

    *Vu.slc  VV (V receive, V transmit)

    *Vl.slc  HV (H receive, V transmit)

2. Run second time with gpri2_proc.py in -t TX_ANTENNA mode to H

    *Hu.slc  VH (V receive, H transmit)

    *Hl.slc  HH (H receive, H transmit)

a)  b) 

**Figure 2.8**. Photos illustrate various connections and setup of the GBIR polarimetric mode. a) C-band RF unit connections are identified. b) C-band 2-m dual-polarized antennas are shown mounted on the GBIR tower.

Images may be acquired line by line by azimuthally rotating the GBIR antennas about the vertical axis. The antennas may be tilted vertically up or down to illuminate the desired area. The GBIR system can radiate microwaves at different frequencies, including C-band with a center frequency of 5.4 GHz and Ku-band with a center frequency of 17.2 GHz. The radar frequencies allow high sensitivity to motion in a number of varying scenarios. The fully polarimetric capabilities of MU GBIR system enable the application of polarimetric interferometry, scatterer decomposition, and other advanced polarimetric methods. The instrument is portable and may be battery operated. When employing an azimuth scan, a data collect may be accomplished in about 20 seconds for a 180 degree sweep.

Another distinct advantage of MU GBIR system lies in that this portable instrument may be removed and repositioned at the same point with high geodetic-grade precision. The standard setup of the GBIR system takes about 10 minutes and is reproducible. Repeated field experiments can be performed at the same point with the help of the provided laser plummet on the instrument, GPS, and other known markers.

**Table 2-1**. GBIR Specification Summary.

| **Type** | **C-Band Specification** | **Ku-band Specification** |
|---|---|---|
| Radar Type | FM-CW, chirps between 0.25 to 8 ms | FM-CW, chirps between 0.25 to 8 ms |
| Radar Modes | Fully Polarimetric (HH,HV,VH, and VV)<br>Single Polarization (HH,HV,VH, or VV)<br>Interferometric | Single Polarization 2m Antenna (VV)<br>Single Polarization Horn (HH,HV,VH, or VV)<br>Interferometric |
| Transmit Power | 100 mW (+20 dBm) | 100 mW (+20 dBm) |
| Chirp Bandwidth | 200 MHz | 200 MHz |
| Azimuth Scan Time | 20 sec for 180 degree sweep | 20 sec for 180 degree sweep |
| ADC | 14-bit, dual channel, 6.25 MHz sample clock | 14-bit, dual channel, 6.25 MHz sample clock |

**Table 2-2**. GBIR 2m Antenna Instrument Specification Summary.

| **Type** | **C-Band Specification** | **Ku-band Specification** |
|---|---|---|
| Frequency | 5.3 to 5.5 GHz | 17.1 to 17.3 GHz |
| 2m Antenna Pattern | 1.5 degree, 3 dB Azimuth Beamwidth<br>38 degree, 3 dB Elevation Beamwidth<br>Peak sidelobes: -13 dB sidelobes (1-way) | 0.5 degree, 3 dB Azimuth Beamwidth<br>38 degree, 3 dB Elevation Beamwidth<br>Peak sidelobes: -15 dB sidelobes (1-way) |
| Antenna Polarization | Dual Polarized (H and V) | Single Polarization (V) |
| Radar operational Range | 10 m – 10 km | 10 m – 10 km |
| Azimuth Resolution | ~26 m at 1 km, proportional to slant range | ~9 m at 1 km, proportional to slant range |
| Range Resolution | 0.75 m without weighting<br>1.0 m with Kaiser Weighting | 0.75 m without weighting<br>1.0 m with Kaiser Weighting |

**Table 2-3**. GBIR Horn Antenna Instrument Specification Summary.

| **Type** | **C-Band Specification** | **Ku-band Specification** |
|---|---|---|
| Frequency | 5.3 to 5.5 GHz | 17.1 to 17.3 GHz |
| Horn Antenna Pattern | ~35 degree, 3 dB Azimuth Beamwidth<br>~35 degree, 3 dB Elevation Beamwidth<br>Peak sidelobes: -10 dB sidelobes (1-way) | ~10 degree, 3 dB Azimuth Beamwidth<br>~20 degree, 3 dB Elevation Beamwidth<br>Peak sidelobes: -10 dB sidelobes (1-way) |
| Antenna Polarization | Dual Polarized (H and V) | Dual Polarized (H and V) |
| Radar operational Range | < 500 m | < 500 m |
| Azimuth Resolution | ~ 31 m at 50 m, proportional to slant range | ~9 m at 50 m, proportional to slant range |
| Range Resolution | 0.75 m without weighting<br>1.0 m with Kaiser Weighting | 0.75 m without weighting<br>1.0 m with Kaiser Weighting |

# CHAPTER 3: GBIR POLARIMETRIC METHODOLGIES

## 3.1 RADAR Polarimetry Overview

In RADAR polarimetry, information is transmitted from the scatterer to the RADAR sensor by EM waves. An EM plane wave's amplitude, phase, and polarization contain information [van Zyl and Kim, 2011]. Polarimetric RADARs measure the full scattering matrix. The received voltage may be written [van Zyl and Kim, 2011] as

$$V = c_a \mathbf{p}^{rec} \cdot [\mathbf{S}]\mathbf{p}^{tr} \tag{3.1}$$

where $\mathbf{p}^{rec}$, $\mathbf{p}^{tr}$ are the normalized receiving and transmitting polarization vectors and **S** is the scattering matrix given by

$$[\mathbf{S}] = \begin{pmatrix} S_{hh} & S_{hv} \\ S_{vh} & S_{vv} \end{pmatrix} \tag{3.2}$$

where the first subscript refers to receiving polarization and the second subscript refers to transmitting polarization. Examination of equation 3.1 reveals that two components of the scattering matrix may be measured at a time by setting one transmit vector element to 1 and the other to 0 such as the following,

$$\begin{pmatrix} S_{hh} \\ S_{vh} \end{pmatrix} = \begin{pmatrix} S_{hh} & S_{hv} \\ S_{vh} & S_{vv} \end{pmatrix} \begin{pmatrix} 1 \\ 0 \end{pmatrix}^{tr} \tag{3.3}$$

$$\begin{pmatrix} S_{hv} \\ S_{vv} \end{pmatrix} = \begin{pmatrix} S_{hh} & S_{hv} \\ S_{vh} & S_{vv} \end{pmatrix} \begin{pmatrix} 0 \\ 1 \end{pmatrix}^{tr} \tag{3.4}$$

Polarimetric data may be acquired by pulse interleaving H and V transmitting pulses and receiving both H and V as shown in Figure 3.1 [Elachi and van Zyl, 2006].

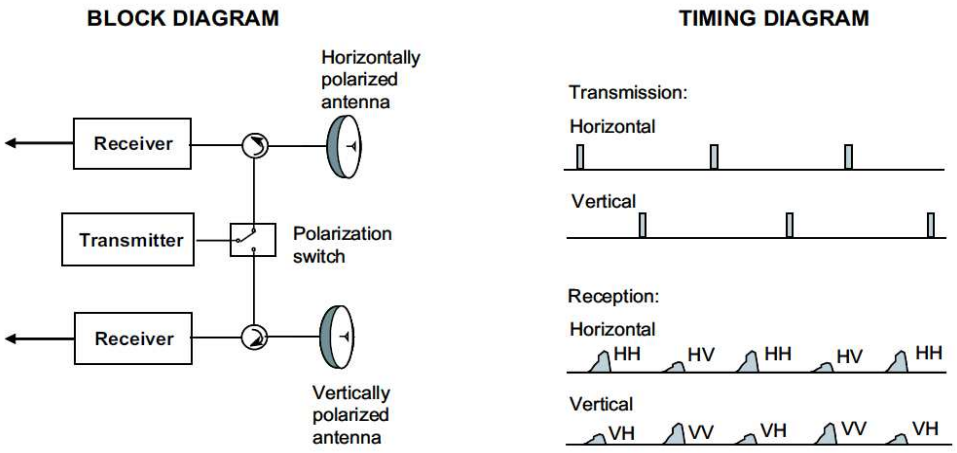


**Figure 3.1**. Diagram illustrates polarimetric RADAR measurement concept [Elachi and van Zyl, 2006].

A number of calibration techniques exist for polarimetric RADAR. Absolute calibration corrects a number amplitude and phase errors. Absolute calibration (i.e. discussed in section 3.2) typically uses known targets such trihedral corner reflectors, spheres, and certain distributed targets [Papathanassiou and Zink, 1998]. Crosstalk calibration (discussed in section 3.3) [Quegan, 1994] may be done before [e.g. Papathanassiou and Zink, 1998] or after absolute calibration [e.g. Fore *et al*., 2009].

For fully polarimetric RADAR measurements, effects from antenna crosstalk, absolute amplitude error, and absolute phase errors may be modeled [van Zyl and Kim, 2011; Papathanassiou and Zink, 1998 ; Quegan, 1994] as

$$[O] = Y[R_x][R_i][S][R_i][R_t] + [N_t] \tag{3.5}$$

where $[R_x]$ describes the polarization impurity on receive normalized to receive channel imbalance, $[R_t]$ describes the polarization impurity on transmit normalized to receive channel imbalance, $[R_i]$ describes the receive channel imbalances, and $[N_t]$ is the noise. Equation 3.5 may be expanded and rewritten in the following form as

$$[O] = Y\begin{bmatrix}1 & w\\ u & 1\end{bmatrix}\begin{bmatrix}k & 0\\ 0 & 1\end{bmatrix}[S]\begin{bmatrix}k & 0\\ 0 & 1\end{bmatrix}\begin{bmatrix}\alpha & \alpha z\\ v & 1\end{bmatrix} + [N_t] \tag{3.6}$$

where $Y$ is the overall system gain in the channel 2 (i.e. V channel here), $k$ is the receive channel imbalance, $\alpha$ is the ratio of transmit and receive channel imbalances, and the crosstalk ratios are $u$, $v$, $w$, and $z$. The observed scattering matrix elements (i.e. vector $O$) may be related to the actual scattering matrix elements (i.e. vector $S$) using the following form of the model as

$$\begin{pmatrix}O_{hh}\\ O_{vh}\\ O_{hv}\\ O_{vv}\end{pmatrix} = Y\begin{pmatrix}1 & w & v & vw\\ u & 1 & uv & v\\ z & wz & 1 & w\\ uz & z & u & 1\end{pmatrix}\begin{pmatrix}\alpha & 0 & 0 & 0\\ 0 & \alpha & 0 & 0\\ 0 & 0 & 1 & 0\\ 0 & 0 & 0 & 1\end{pmatrix}\begin{pmatrix}k^2 & 0 & 0 & 0\\ 0 & k & 0 & 0\\ 0 & 0 & k & 0\\ 0 & 0 & 0 & 1\end{pmatrix}\begin{pmatrix}S_{hh}\\ S_{vh}\\ S_{hv}\\ S_{vv}\end{pmatrix} + \begin{pmatrix}N_{t,hh}\\ N_{t,vh}\\ N_{t,hv}\\ N_{t,vv}\end{pmatrix} \tag{3.7}$$

In this chapter, the scattering matrix elements may form uncalibrated RCS elements by squaring the absolute value of the scattering matrix elements unless noted otherwise. Uncalibrated sigma nought values may be obtained by dividing the uncalibrated RCS elements by the area illuminated.

### 3.2 Crosstalk Calibration Before Absolute Calibration

Using the scattering measurement model of equation 3.5 [Quegan, 1994], the crosstalk effects due to the matrices $[R_x]$ and $[R_t]$ may be reduced. Using equation 3.7 and equation 3.5, the observed scattering matrix may be written as

$$[O] = [R_x][S'][R_t] + [N_t] \quad . \tag{3.8}$$

In vector form, equation 3.8 may be written as

$$\begin{pmatrix} O_{hh} \\ O_{vh} \\ O_{hv} \\ O_{vv} \end{pmatrix} = [D] \begin{pmatrix} S'_{hh} \\ S'_{vh} \\ S'_{hv} \\ S'_{vv} \end{pmatrix} + \begin{pmatrix} N_{t,hh} \\ N_{t,vh} \\ N_{t,hv} \\ N_{t,vv} \end{pmatrix} \tag{3.9}$$

where [$D$] is the crosstalk matrix. Using equation 3.7, the crosstalk matrix may be written as

$$[D] = \begin{pmatrix} 1 & w & v & vw \\ u & 1 & uv & v \\ z & wz & 1 & w \\ uz & z & u & 1 \end{pmatrix} \begin{pmatrix} \alpha & 0 & 0 & 0 \\ 0 & \alpha & 0 & 0 \\ 0 & 0 & 1 & 0 \\ 0 & 0 & 0 & 1 \end{pmatrix} = \begin{pmatrix} \alpha & \alpha w & v & vw \\ \alpha u & \alpha & uv & v \\ \alpha z & \alpha wz & 1 & w \\ \alpha uz & \alpha z & u & 1 \end{pmatrix} \tag{3.10}$$

The scattering matrix with crosstalk reduction may be written as

$$[S'] = [R_x]^{-1}([O] - [N_t])[R_t]^{-1} = [P]([O] - [N_t]) \tag{3.11}$$

where [$P$] is the crosstalk calibration matrix. The crosstalk calibration matrix [Papathanassiou and Zink, 1998] may be written as

$$[P] = [D]^{-1} = \frac{1}{\alpha(uw-1)(vz-1)} \begin{pmatrix} 1 & -w & -v & vw \\ -u & 1 & uv & -v \\ -\alpha z & \alpha wz & \alpha & -\alpha w \\ \alpha uz & -\alpha z & -\alpha u & \alpha \end{pmatrix} \tag{3.12}$$

The crosstalk ratios (i.e. $u$, $v$, $w$, and $z$) and the ratio of receive channel to transmit channel imbalance (i.e. $\alpha$) may be found according in the literature [Quegan, 1994], and a brief summary follows. Here, the crosstalk reduction method is a unified approach to cross-talk calibration of distributed target parameters or scattering matrix data in

polarimetric SAR images [Quegan, 1994]. It is a direct and non-iterative calibration technique that is applicable to calibrating distributed targets or complex data. The application of this calibration procedure is subject to certain model assumptions. Distributed targets can be used in order to perform crosstalk calibration on the basis of two kinds of assumptions (i.e. target and system) [Quegan, 1994] as listed in Table 3-1.

Table 3-1. Crosstalk calibration assumptions are listed [Quegan, 1994].

| Assumption Number | Assumption Type | Assumption Summary |
|---|---|---|
| 1. | Target | Every pixel in the distributed target has a 2 x 2 complex scattering matrix $S$, where $S_{ij}$ is the response in the polarization state $i$ from a stimulus in polarization state $j$. |
| 2. | Target | The reciprocity principle states that $S_{hv} = S_{vh}$, unless the target's physical state is altered by radar illumination. This need not be true for all targets but if it is, then we can equate the scattering matrix $S$ with a 4-vector $S = (S_{hh}, S_{vh}, S_{hv}, S_{vv})^t$. |
| 3. | Target | The scene is dominated by distributed targets for which the true like and cross-polarized returns are uncorrelated, (i.e.,$\langle S_{ji} S_{ij}^* \rangle = 0$ if $j \neq i$ where $\langle . \rangle$ denotes expectation). This assumption is based on the expectation that most natural targets display azimuthal symmetry. |
| 4. | System | The system effects can be modeled by a two-stage linear process so that the observed data matrix O can be written as $[O] = [R_x][S'][R_t] + [N_t]$. |
| 5. | System | The matrices $[R_r]$ and $[R_t]$ have off-diagonal (cross-talk) terms $r_{ij}$ and $t_{ij}$, where $i \neq j$, which are small compared to the diagonal terms $r_{ii}$ and $t_{ii}$. |

From assumptions 1, 2, and 3, the scene is dominated by targets with the scatterer covariance written as

$$C_s = S_s S_s^{*T} = \begin{pmatrix} \sigma_{hh} & 0 & 0 & \rho \\ 0 & \sigma_{vh} & \sigma_{vh} & 0 \\ 0 & \sigma_{vh} & \sigma_{vh} & 0 \\ \rho^* & 0 & 0 & \sigma_{vv} \end{pmatrix} \tag{3.13}$$

where $S_s = (S_{hh,s}, S_{vh,s}, S_{hv,s}, S_{vv.s})$ and $\rho = < S_{hh,s} S_{vv.s}{}^* >$. By neglecting noise, the averaged observed scatterer covariance matrix may be written as

$$\langle C_O \rangle = \langle O_s O_s^{*T} \rangle = [D]\langle [C_s] \rangle [D]^{*T} = \begin{pmatrix} C_{11} & C_{12} & C_{13} & C_{14} \\ C_{21} & C_{22} & C_{23} & C_{24} \\ C_{31} & C_{32} & C_{33} & C_{34} \\ C_{41} & C_{42} & C_{43} & C_{44} \end{pmatrix} \tag{3.14}$$

where $O_s = (O_{hh,s}, O_{vh,s}, O_{hv,s}, O_{vv,s})$. The crosstalk ratios (i.e. $u$, $v$, $w$, and $z$) and the ratio of receive channel to transmit channel imbalance (i.e. $\alpha$) may be written as

$$u = \frac{C_{44}C_{21} - C_{41}C_{24}}{\Delta} \tag{3.15}$$

$$v = \frac{C_{11}C_{24} - C_{21}C_{14}}{\Delta} \tag{3.16}$$

$$z = \frac{C_{44}C_{31} - C_{41}C_{34}}{\Delta} \tag{3.17}$$

$$w = \frac{C_{11}C_{34} - C_{31}C_{14}}{\Delta} \tag{3.18}$$

$$\alpha = |\alpha| arg(\alpha) \tag{3.19}$$

where

$$|\alpha| = \frac{|\alpha_1\alpha_2| - 1\sqrt{(|\alpha_1\alpha_2| - 1)^2 + 4|\alpha_2|^2}}{2|\alpha_2|} \tag{3.20}$$

$$arg(\alpha) = -arg(X) \tag{3.21}$$

$$\Delta = C_{11}C_{44} - |C_{14}|^2 \tag{3.22}$$

$$\alpha_1 = \frac{C_{22} - uC_{12} - vC_{42}}{X} \tag{3.23}$$

$$\alpha_2 = \frac{X^*}{C_{33} - z^*C_{31} - w^*C_{34}} \tag{3.24}$$

$$X = C_{32} - zC_{12} - wC_{42} \quad . \tag{3.25}$$

To account for fluctuations, the parameters may be averaged over incident angle, range, small local regions, or globally. The method may calibrate regions for which the assumptions are invalid by using the parameters that are derived from the global behavior of pixels that meet the method assumptions [Quegan, 1994]. After crosstalk calibration, the resulting scattering matrix [*S'*] may further calibrated by absolute calibration (e.g. section 3.3).

### 3.3 Absolute Calibration

Absolute calibration of polarimetric RADAR is thoroughly covered in the literature. Here, one absolute calibration methodology using trihedral corner reflectors is summarized from the literature [Fore *et al.*, 2009]. By neglecting antenna and crosstalk effects in equation 3.5, the polarimetric scattering measurements without absolute amplitude and phase correction may be written as [Fore *et al.*, 2009; Quegan, 1994]

$$[S'] = Y[R_i][S][R_i] \tag{3.25}$$

or as

$$\mathrm{S}' = \mathrm{A}\begin{bmatrix} S_{hh}expi(\phi_{t,h} + \phi_{r,h}) & S_{hv}fgexpi(\phi_{t,v} + \phi_{r,h}) \\ S_{vh}(\frac{f}{g})expi(\phi_{t,h} + \phi_{r,v}) & S_{vv}f^2expi(\phi_{t,v} + \phi_{r,v}) \end{bmatrix} \tag{3.26}$$

where the real valued variables are as follows: *A* is the absolute calibration error, *f* is the co-polarization channel imbalance, *g* is the cross-polarization channel imbalance, □*t,v* is

the induced phase error while transmitting V-polarization, $\square_{r,v}$ is the induced phase error while receiving V-pol. By removing arbitrary phase from this expression, one may obtain

$$S' = A\begin{bmatrix} S_{hh} & S_{hv}fgexpi\phi_t \\ S_{vh}(\frac{f}{g})expi\ \phi_r) & S_{vv}f^2expi(\phi_t + \phi_r) \end{bmatrix} \tag{3.27}$$

where the phases $\square_t$ and $\square_r$ may be written as

$$\phi_t = \phi_{t,v} - \phi_{t,h} \tag{3.28}$$

$$\phi_r = \phi_{r,v} - \phi_{r,h} \quad . \tag{3.29}$$

In order to estimate the calibration parameters ($\square_t$, $\square_r$, $A$, $f$, and $g$) using trihedral corner reflectors (TCR) and distributed targets, a summary from the literature is provided [Fore *et al.*, 2009]. For the trihedral corner reflector, the scattering matrix is assumed to be of the form

$$S_{tri} = \sqrt{\sigma_{tcr}}\begin{bmatrix} 1 & 0 \\ 0 & 1 \end{bmatrix} \tag{3.30}$$

where $\sigma_{tcr}$ is TCR sigma nought. The TCR sigma nought may be written [Bonkowski *et al.*, 1953] as

$$\sigma_{tcr} = \frac{4\pi l^4}{\lambda^2}\left[\cos\theta_{cr} + \sin\theta_{cr}(\sin\phi_{cr} + \cos\phi_{cr}) - \frac{2}{\cos\phi_{cr}+\sin\theta_{cr}(\sin\phi_{cr}+\cos\phi_{cr})}\right]^2 \tag{3.31}$$

where $l$ is the length of the short sides of the TCR, $\lambda$ is the radar wavelength, and $\theta_{cr}$ is the incident angle, $\square_{cr}$ is the azimuth angle as shown in Figure 3.2.

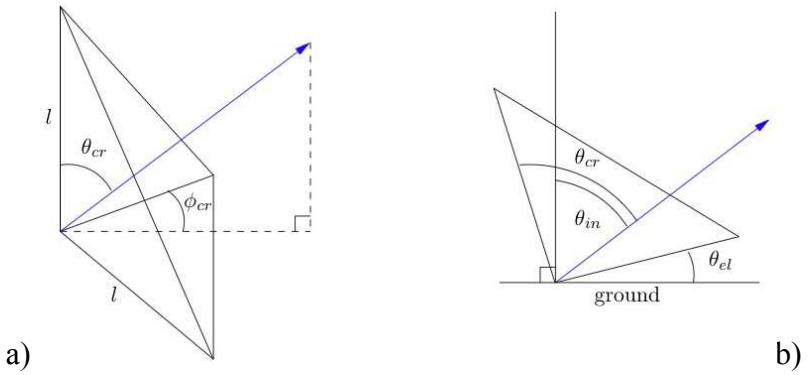


a) b)

**Figure 3.2**. TCR geometry is illustrated. a) Azimuth orientation is shown. b) Elevation orientation is shown. The blue vector points toward the RADAR. The incidence angle relative to the corner reflector is $\theta_{cr}$ is the incidence angle relative to the TCR, $\theta_{in}$ is the incidence angle, and $\theta_{el}$ is the elevation angle of the TCR relative to the ground, $\phi_{cr}$ is the azimuth angle relative to one of the vertical sides of the TCR [Fore *et al.*, 2009].

The observed scattering matrix at the corner reflector may be written as

$$S'_{tcr} = \begin{bmatrix} S'_{hh} & S'_{hv} \\ S'_{vh} & S'_{vv} \end{bmatrix} = A\sqrt{\sigma_{tcr}} \begin{bmatrix} 1 & 0 \\ 0 & f^2 expi(\phi_t + \phi_r) \end{bmatrix} \quad . \tag{3.32}$$

To estimate the absolute calibration parameter A, the average off set between the predicted RCS and the measured RCS may found from the following as

$$\langle 10\, log_{10}\left[\sigma_{tcr,i}/\langle S'_{hh,i} S'^{*}_{hh,i}\rangle_{TCR\,i}\right]\rangle_{all\,TCR} = -10\, log_{10} A^2 \tag{3.33}$$

or

$$A = \sqrt{10^{-\frac{\langle 10\, log_{10}\left[\sigma_{tcr,i}/\langle S'_{hh,i} S'^{*}_{hh,i}\rangle_{TCRi}\right]\rangle_{allTCR}}{10}}} \tag{3.34}$$

where $\langle\rangle_{TCRi}$ is the average over pixels associated with TCR number *i*, *allTCR* is the average over all the TCRs, and $\sigma_{tcr,I}$ is the *TCRi*'s scattering coefficient.

From equation 3.32, the average estimate for the co-polarization channel imbalance, *f*, from the TCRs may written as

$$f = \left( \langle \langle \frac{S'_{vv} S'^{*}_{vv}}{S'_{hh} S'^{*}_{hh}} \rangle_{TCRi} \rangle_{allTCR} \right)^{\frac{1}{4}} \tag{3.35}$$

To obtain the cross-polarization channel imbalance, the averages of HV and VH power over a large number of pixels from distributed targets (DT) (i.e. $\langle\rangle_{DT}$) are computed [Fore et. al, 2009]; therefore, cross-polarization imbalance, *g*, can be written as

$$g = \left( \frac{\langle |S'_{hv}|^2 \rangle_{DT}}{\langle |S'_{vh}|^2 \rangle_{DT}} \right)^{\frac{1}{4}} \quad . \tag{3.36}$$

For the phase calibration of the co-polarization channels, the parameters ($\phi_t + \phi_r$) and ($\phi_t - \phi_r$) may be computed. From equation 3.32, ($\phi_t + \phi_r$) may be estimated for each TCR at its incident angle ($\theta_{inc,i}$) as

$$\phi_{t,i} + \phi_{r,i} = \arg\left( \langle S'_{vv} S'^{*}_{hh} \rangle_{TCRi} \right) \text{ for } \theta_{inc,i} \tag{3.37}$$

then applied to a least-squares fit of the model written as

$$\phi_t(\theta_{inc}) + \phi_r(\theta_{inc}) = a_{\phi_t + \phi_r} + b_{\phi_t + \phi_r}(\theta_{inc} - 45^o) \tag{3.38}$$

where $a_{\phi t+\phi r}$ and $b_{\phi t+\phi r}$ are the model coefficients (i.e. phase bias and slope). For phase calibration of the cross-polarization channels the expectation is reciprocity (i.e. $S_{vh}$ equals $S_{hv}$) for distributed targets, the parameter ($\phi_t - \phi_r$) may be estimated as

$$\phi_t - \phi_r = \arg(< S'_{hv} S'^{*}_{vh} >_{DT}) \tag{3.39}$$

Thus, the scattering matrix of equation 3.27 may be calibrated using the absolute and phase calibration parameters ($A$, $f$, $g$, $\Box_t + \Box_r$ per TCR, $\Box_t + \Box_r$ per incident angle, $\Box_t - \Box_r$) found in equations 3.34, 3.35, 3.36, 3.37, 3.38, and 3.39 [Fore *et al.*, 2009].

### 3.4 Crosstalk Calibration after Absolute Calibration

The observed scattering matrix [$O$] may be absolute calibrated (e.g. section 3.3) before crosstalk removal. The absolute calibrated observed scattering may be written as

$$[O_{after}] = \begin{pmatrix} O_{hh} \\ O_{vh} \\ O_{hv} \\ O_{vv} \end{pmatrix}_{after} = [D_{after}] \begin{pmatrix} S_{hh} \\ S_{vh} \\ S_{hv} \\ S_{vv} \end{pmatrix} + \begin{pmatrix} N_{t,hh} \\ N_{t,vh} \\ N_{t,hv} \\ N_{t,vv} \end{pmatrix}_{after} \tag{3.40}$$

where [$D_{after}$] may be found by assuming $Y = 1$ and $k = \alpha^{-0.5}$ [Fore *et al.*, 2009]

for [$O_{after}$] as

$$[D_{after}] = (1) \begin{pmatrix} 1 & w & v & vw \\ u & 1 & uv & v \\ z & wz & 1 & w \\ uz & z & u & 1 \end{pmatrix} \begin{pmatrix} \alpha & 0 & 0 & 0 \\ 0 & \alpha & 0 & 0 \\ 0 & 0 & 1 & 0 \\ 0 & 0 & 0 & 1 \end{pmatrix} \begin{pmatrix} 1/\alpha & 0 & 0 & 0 \\ 0 & 1/\sqrt{\alpha} & 0 & 0 \\ 0 & 0 & 1/\sqrt{\alpha} & 0 \\ 0 & 0 & 0 & 1 \end{pmatrix} = \begin{pmatrix} 1 & w\sqrt{\alpha} & v/\sqrt{\alpha} & vw \\ u & \sqrt{\alpha} & uv/\sqrt{\alpha} & v \\ z & wz\sqrt{\alpha} & 1/\sqrt{\alpha} & w \\ uz & z\sqrt{\alpha} & u/\sqrt{\alpha} & 1 \end{pmatrix} \tag{3.41}$$

and the crosstalk calibration matrix for the absolute calibrated observed scattering matrix may be written as

$$[P_{after}] = [D_{after}]^{-1} = \frac{1}{(uw-1)(vz-1)} \begin{pmatrix} 1 & -w & -v & vw \\ -u/\sqrt{\alpha} & 1/\sqrt{\alpha} & uv/\sqrt{\alpha} & -v/\sqrt{\alpha} \\ -z\sqrt{\alpha} & wz\sqrt{\alpha} & \sqrt{\alpha} & -w\sqrt{\alpha} \\ uz & -z & -u & 1 \end{pmatrix} \tag{3.42}$$

such that

$$[S] = [P_{after}]([O_{after}] - [N_{t,after}]) \quad . \tag{3.43}$$

*3.4.1 Example Crosstalk Effect on Signal Phase*

The standard deviation of the phase error for a signal with crosstalk having a uniform phase may be written as

$$\varepsilon(CR) \approx stdev\left(arg\left(1 + CR * e^{iU(-\pi,\pi)}\right)\right) \tag{3.44}$$

where *CR* is the amplitude crosstalk ratio (i.e. values 0 to 1), and $U(-\pi,\pi)$ is a uniform phase distribution over the range $-\pi$ to $\pi$, the desired signal's amplitude is one with zero phase, and the undesired signal's amplitude is one before cross talking occurs. Figure 3.3 shows an example from runs using 100000 samples each for various amplitude crosstalk ratios.

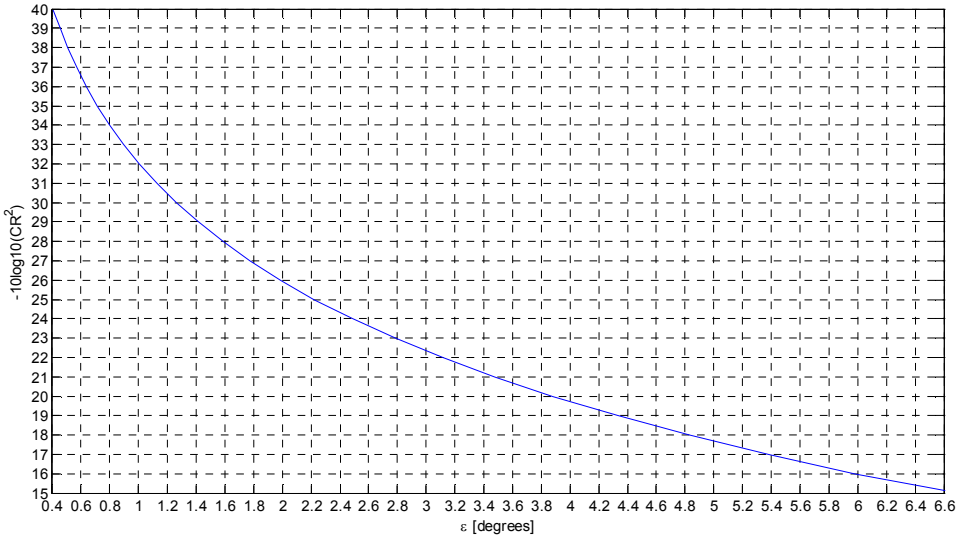


**Figure 3.3**. Phase error standard deviation is shown.

## 3.5 Data Culling

Before crosstalk calibrating an array of observed scattering matrix data, the data may be checked for model and method ill conditions. The parameters estimated during crosstalk calibration may be averaged to find global values (e.g. range, incident angle, etc.). Culling or pruning out ill conditioned data allows these global estimates to be calculated according to the methods in section 3.2 and 3.4.

Condition image masks are formed such that each mask pixel is either one (i.e. passes acceptable condition) or zero (i.e. fails acceptable condition). By combining all the condition masks, a total mask may be formed. An element in the total mask will be one only if all the corresponding elements in the condition masks are one; otherwise, the element is zero. Only observed scattering locations with total mask value of one will be used in the crosstalk computation (e.g. covariance matrices average window, $C_O$, $u$, $v$, $z$, $w$, $\alpha$, etc.).

### *3.5.1 High HH-HV Correlation*

From assumption 3 (i.e. Table 3-1), the distributive targets are expected to be of low HH-HV correlation. The level of crosstalk can increase the correlation. Nevertheless, correlations over a window, $W_{ccf}$, that exceed a value, $T_{ccf}$, may be culled from crosstalk estimations. The HH-HV correlation may be written as

$$|\rho_{13}| = \left| \frac{\langle O_{hh} O_{hv}^* \rangle}{\sqrt{\langle O_{hh} O_{hh}^* \rangle \langle O_{hv} O_{hv}^* \rangle}} \right| \quad . \tag{3.45}$$

The high correlation mask may be formed as

$$M_{ccf} = \begin{cases} 1 & |\rho_{13}| < T_{ccf} \\ 0 & |\rho_{13}| \geq T_{ccf} \end{cases} \quad . \tag{3.46}$$

*3.5.2 Low Cross-Polarization Power*

From assumption 1 and method equations [Quegan, 1994], low cross-polarization power may result in unsuccessful crosstalk estimation. The observed cross-polarization power calculated over a window, $W_{cp}$, that exceed a value, $T_{cp}$, may be culled from crosstalk estimations. The observed cross-polarization power (i.e. here sigma nought) may be written as

$$P_{cp} = 10 \log_{10} \langle \frac{O_{hv} O_{hv}^*}{A_{ill}} \rangle \tag{3.47}$$

The low cross-polarization power mask may be formed as

$$M_{cp} = \begin{cases} 0 & P_{cp} \leq T_{cp} \\ 1 & P_{cp} > T_{cp} \end{cases} \tag{3.48}$$

*3.5.3 Culling Mask*

Each condition mask may be combined into a single total mask as

$$M_{tot} = M_{ccf} M_{cp} \tag{3.49}$$

where the multiplication is element by element. Only observed scattering locations with total mask value of one will be used in the crosstalk computation (e.g. covariance matrices average window, $C_O$, $u$, $v$, $z$, $w$, $\alpha$, etc.).

# 4. BLUE SPRINGS DAM SITE DESCRIPTION

The aim of experiments at the Blue Springs Dam site is to monitor the intake tower and embankment. This is currently performed with tilt plate devices. Embankment movement is typically monitored using alignment monuments, crest centerline surveys and foundation settlement plates. According to past surveys, the embankment movement has been relatively minimal in the last 10 yrs. The site is located nearly 120 miles away from University of Missouri-Columbia.

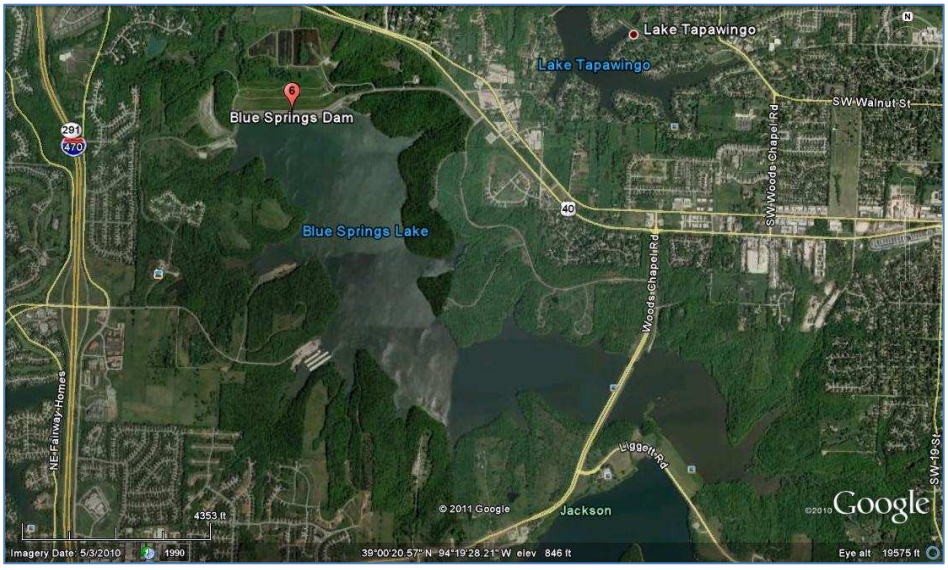


**Figure 4.1**. Image illustrates the area about Blue Springs Dam, MO [Google Earth v6.2].

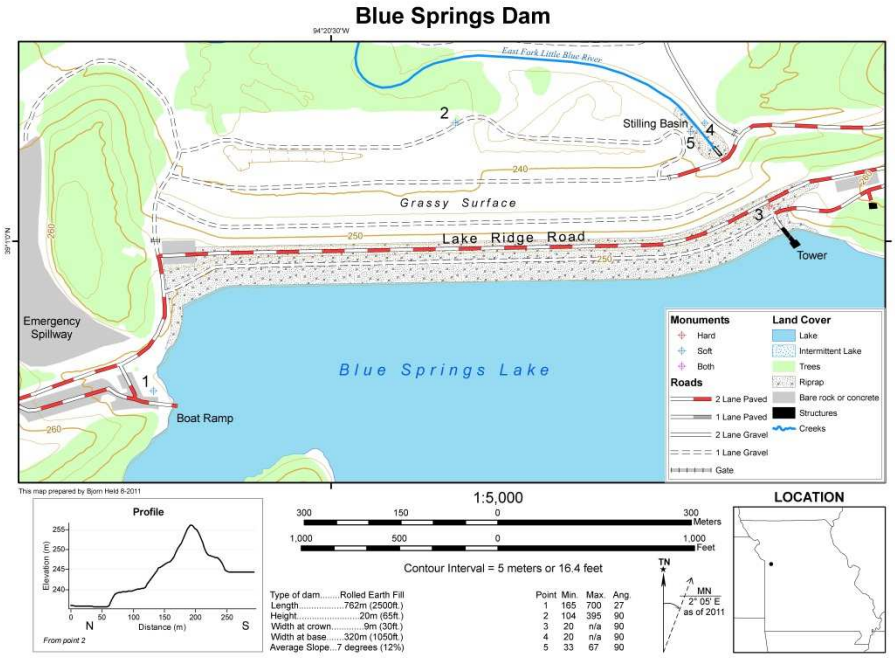


**Figure 4.2**. Monuments distribution at Blue Springs Dam, MO is illustrated.

**Figure 4.3**. A photograph near pin 3 location at Blue Springs Dam, MO is shown.

# 5. RESULTS AND ANALYSIS

## 5.1 Introduction

C-band polarimetric GBIR data were collected on February 18, 2012 for the Blue Springs Dam and surrounding vicinity. This chapter details the crosstalk and other processing results for the Blue Springs data collection.

Figure 5.1 illustrates the uncalibrated power imagery for various polarizations. From equation 2.13 using a decimation of 91, each azimuth bin is about 1°. Using a 200 MHz bandwidth, the range resolution is about 0.75 m. Various near linear features show curved in the image due to polar coordinate display of the data. By observing the imagery starting on the left side and proceeding to the right, the major features may be segmented as follows: a) a bright band from a grassy rolling topography, b) a dark band near an approximately leveled area with a secondary road, c) a bright band primarily from a grassy surface incline, d) a dark band from a secondary road, e) a bright band mainly from a grass incline leading up to the railing of the primary road upon the dam, and f) a dark portion mainly due to shadowing of the water surface. An apparent strong return produces a horizontal stripe near row 180. Various antenna effects are seen to the right of the dam. In the slope leading up dam, several point-like returns from various physical site markers are observed.

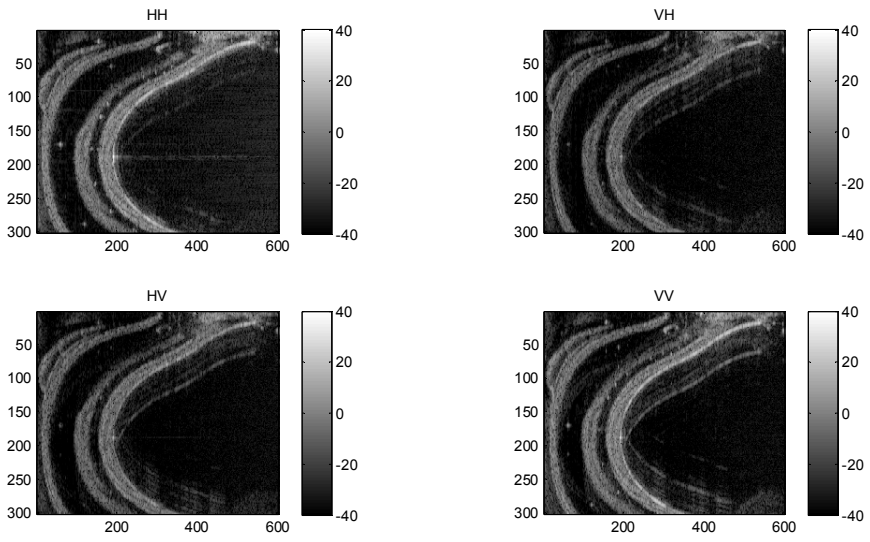


**Figure 5.1**. Blue Springs GBIR data are shown for the polarizations of HH (top left), VH (top right), HV (lower left), and VV (lower right). The images show the signal power in dB. The horizontal scale is slant range bins. The vertical scale is azimuth bins.

## 5.2 Data Culling Yield

To improve the quality of the crosstalk estimations, data points of low quality are removed or masked out with respect to the chapter 3 methodology. To reduce HH-HV correlations greater than or equal to 0.4 using 11 pixels by 11 pixels window centered about each pixel, a mask is formed as shown in Figure 5.2. Various regions of high correlation may be seen as dark in the mask. Pixels with cross-polarization power less than or equal to -20 dB using 11 pixels by 11 pixels window centered about each pixel are removed as shown in Figure 5.3. The grassy areas and incline surfaces are identified while most other shadow and low return locations are masked out. Figure 5.4 illustrates the total mask for the processing flow.

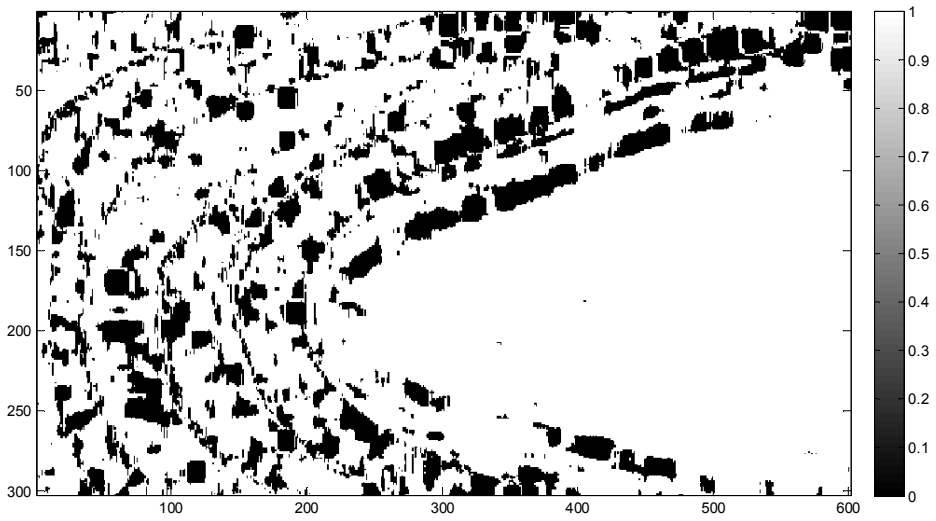


**Figure 5.2.** High HH-HV correlation mask is shown. Mask values of zero are removed from the processing flow. A threshold of 0.4 is used here.

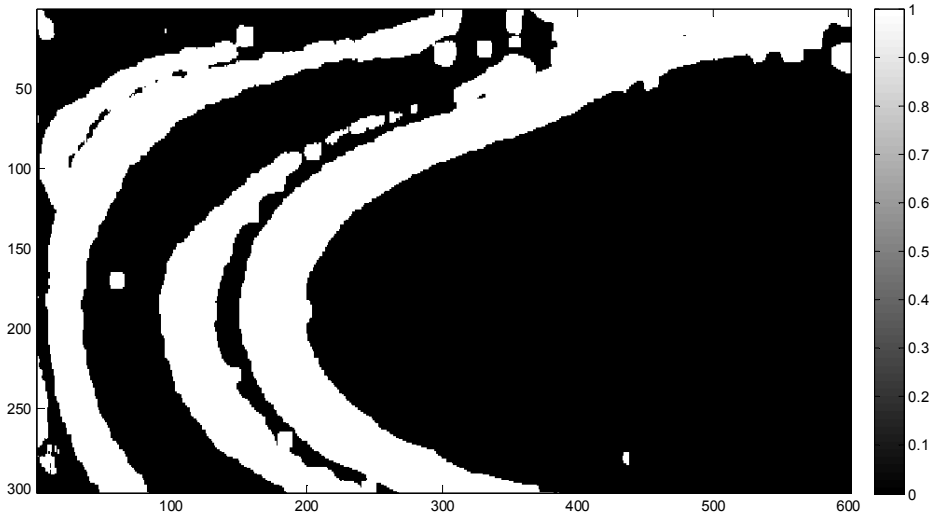


**Figure 5.3.** Low cross-polarization mask is shown. Mask values of zero are removed from the processing flow. A threshold of -20 dB is used here.

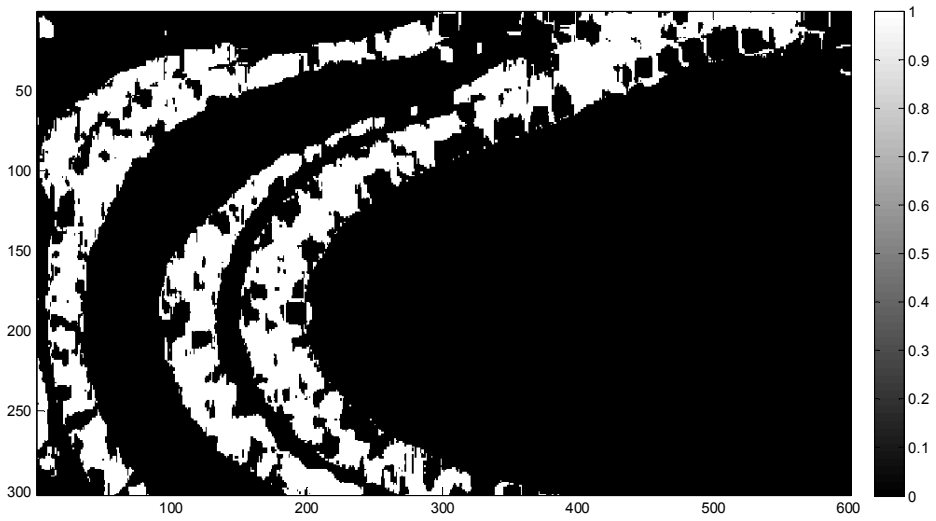


**Figure 5.4**. The total mask is shown. Mask values of zero are removed from the processing flow.

### 5.3 Covariance Matrices

For each pixel, a covariance matrix is formed as described in chapter 3. The covariance matrix elements for each pixel are shown in Figures 5.5 (i.e. real power in dB) and 5.6 (i.e. phase in degrees). After masking, the covariance data are averaged over window of 21 pixels by 21 pixels. The averaged covariance data are shown in Figures 5.7 (i.e. real power in dB) and 5.8 (i.e. phase in degrees). In both cases, unmasked values from the diagonal elements are real (i.e. zero phase) as expected. The covariance elements for combinations of HV and VH are approximately zero (e.g. reciprocity) for the unmasked values. The remaining elements demonstrate a near random phase variation. The crosstalk parameters may be estimated now from the average covariance elements with masking.

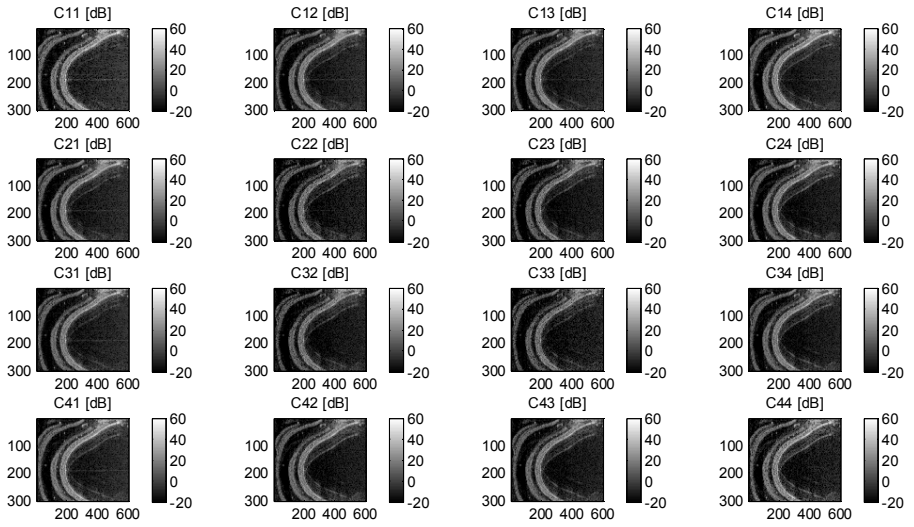


**Figure 5.5**. Initial covariance elements power in dB for each pixel.

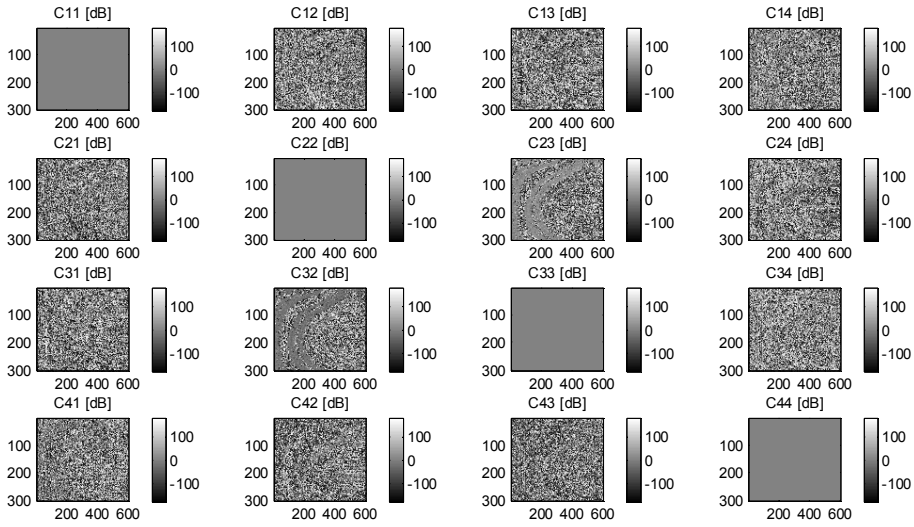


**Figure 5.6**. Initial covariance elements phase in degrees for each pixel.

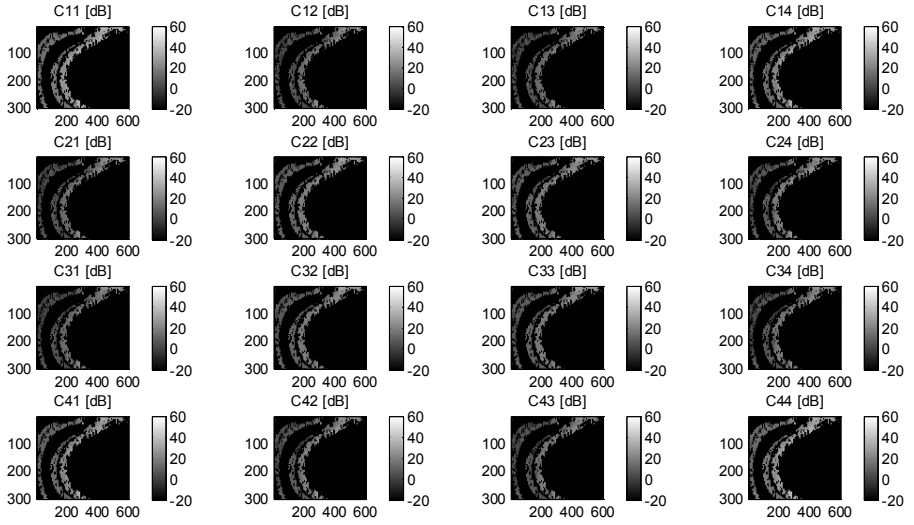


**Figure 5.7**. Averaged covariance elements power in dB for each pixel after data culling.

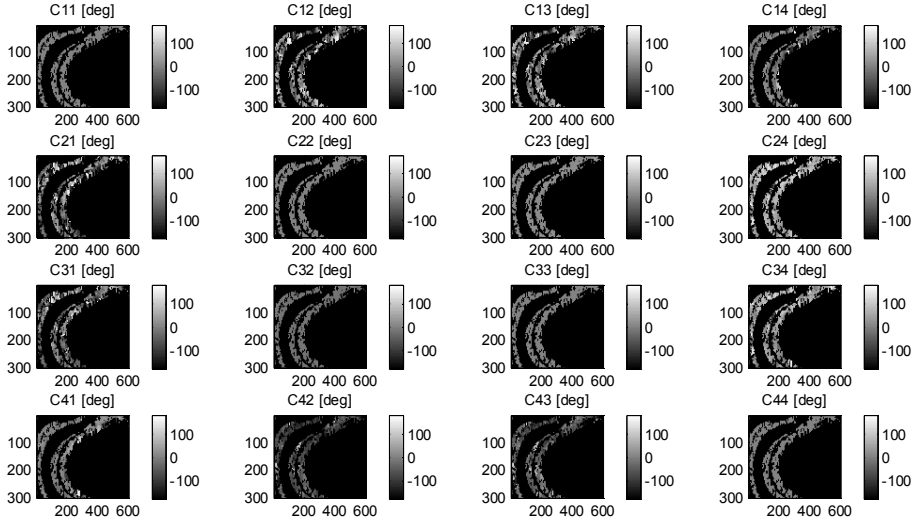


**Figure 5.8**. Averaged covariance elements phase in degrees for each pixel after data culling.

### 5.4 Crosstalk Parameters Results

Using the average covariance matrices of the masked data, the crosstalk ratios (i.e. $u$, $v$, $z$, and $w$) and the ratio of receive channel to transmit channel imbalance (i.e. $\alpha$) were computed for each observed pixel in the processing flow. Figures 5.9 and 5.10 show the results for each unmasked observed pixel. While small fluctuations exist in the crosstalk ratios power, a clear dominant mean is seen for each crosstalk ration of about -25.1 dB, -16.4 dB, -26.5 dB, and -19.9 dB for $u$, $v$, $z$, and $w$, respectively. The phase behavior is similar although a few local regions have significant variation that may perhaps be due to the areas local viewing geometry and scattering. Using equation 3.44, a -16.4 dB crosstalk corresponds to about a 6° standard deviation. The global behavior is used in section 5.5 to crosstalk calibrate the imagery.

After crosstalk calibrating the data, the crosstalk ratios (i.e. $u$, $v$, $z$, and $w$) were calculated and observed for Figures 5.11, 5.12, 5.13, and 5.14. For the crosstalk calibration after absolute calibration method (i.e. eqn. 3.43), a clear dominant mean is seen for each crosstalk ration of about -27.3 dB, -24.8 dB, -26.9 dB, and -24.9 dB. For the crosstalk calibration before absolute calibration method (i.e. eqn. 3.11), a clear dominant mean is seen for each crosstalk ration of about -26.7 dB, -25.3 dB, -26.3 dB, and -25.4 dB. The results from the two methods are similar suggesting that the assumption of $Y$ and $\alpha$ in eqn. 3.43 nearly applied for this data although the data set was not absolutely calibrated before crosstalk calibration. Using equation 3.44, a -25.3 dB crosstalk corresponds to about a 2° standard deviation.

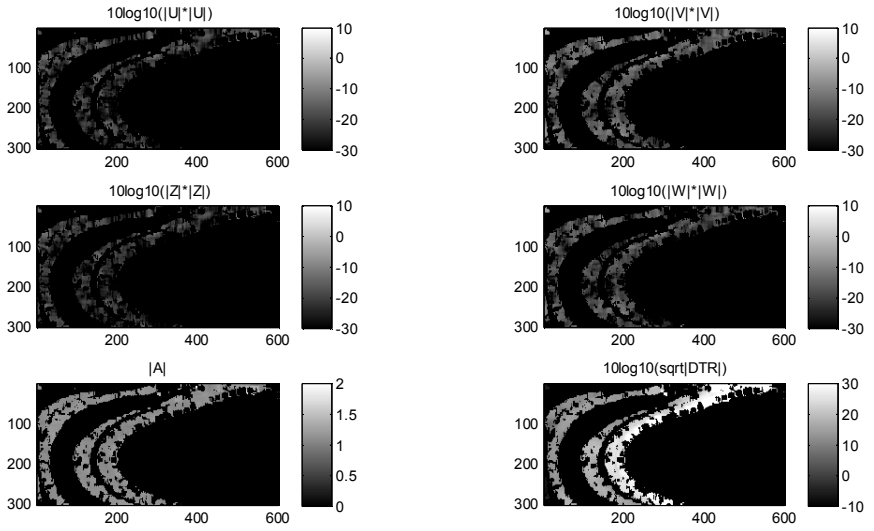


**Figure 5.9**. The observed crosstalk ratios (i.e. *u*, *v*, *w*, and *z*) and the ratio of receive channel to transmit channel imbalance (i.e. $\alpha$) power in dB using the masked average covariance matrices are shown.

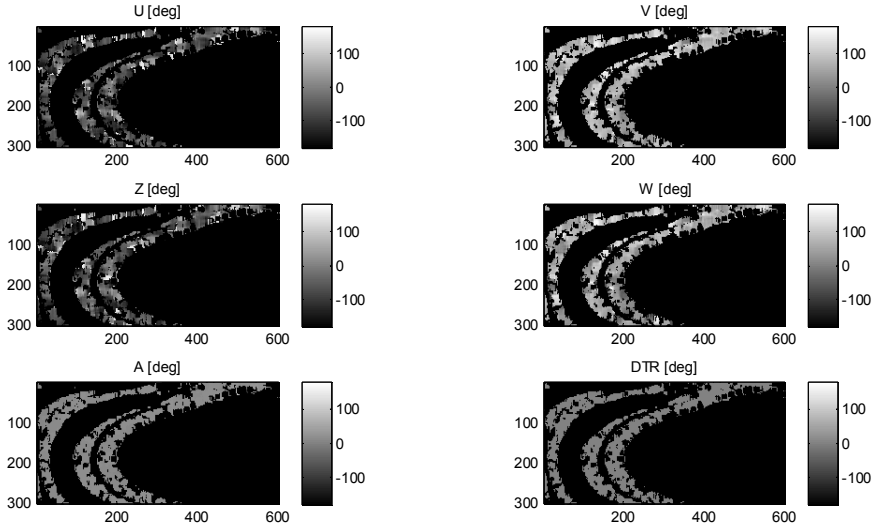


**Figure 5.10**. The observed crosstalk ratios (i.e. *u*, *v*, *w*, and *z*) and the ratio of receive channel to transmit channel imbalance (i.e. $\alpha$) phase in degrees using the masked average covariance matrices are shown.

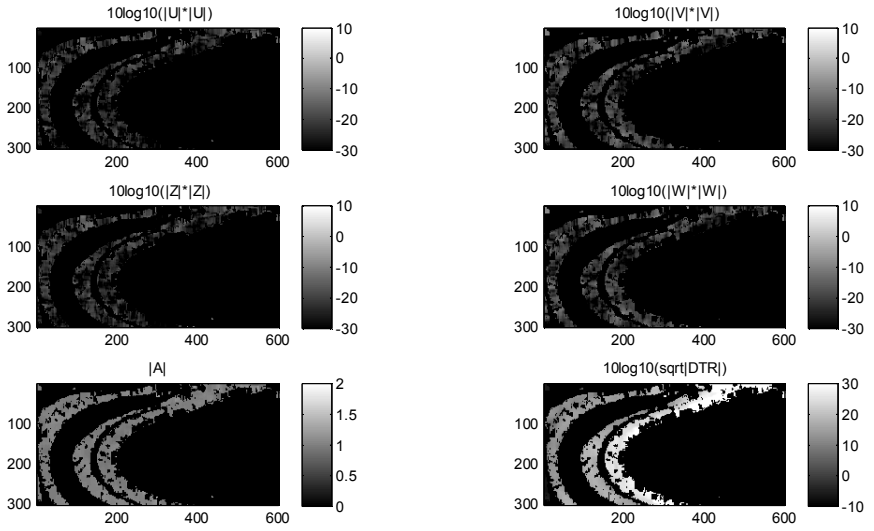


**Figure 5.11**. Results are shown using crosstalk calibration after absolute calibration method. The crosstalk ratios (i.e. *u*, *v*, *w*, and *z*) and the ratio of receive channel to transmit channel imbalance (i.e. $\alpha$) power in dB using the masked average covariance matrices are shown.

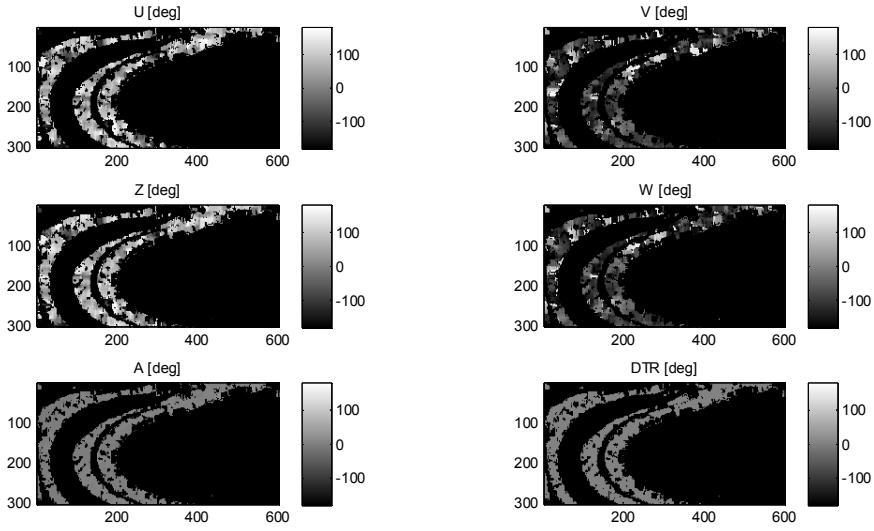


**Figure 5.12**. Results are shown using crosstalk calibration after absolute calibration method. The crosstalk ratios (i.e. *u*, *v*, *w*, and *z*) and the ratio of receive channel to transmit channel imbalance (i.e. $\alpha$) phase in degrees using the masked average covariance matrices are shown.

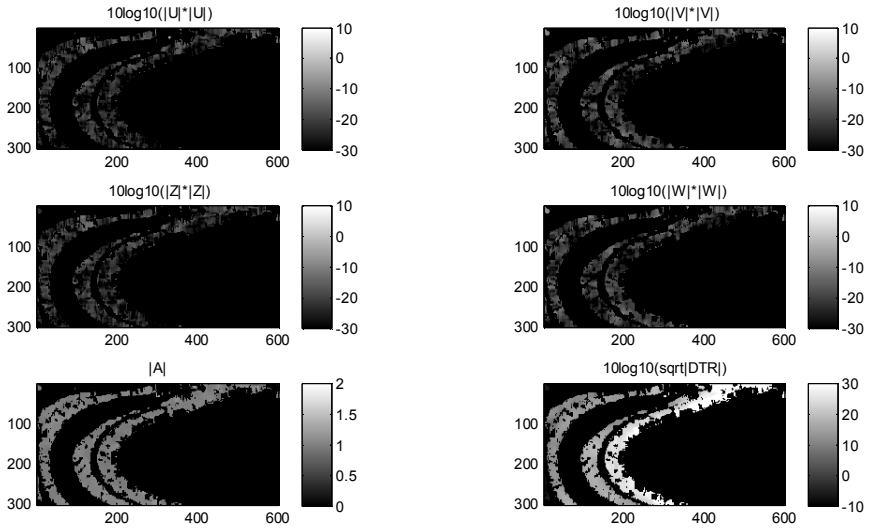


**Figure 5.13**. Results are shown using crosstalk calibration before absolute calibration method. The crosstalk ratios (i.e. $u$, $v$, $w$, and $z$) and the ratio of receive channel to transmit channel imbalance (i.e. $\alpha$) power in dB using the masked average covariance matrices are shown.

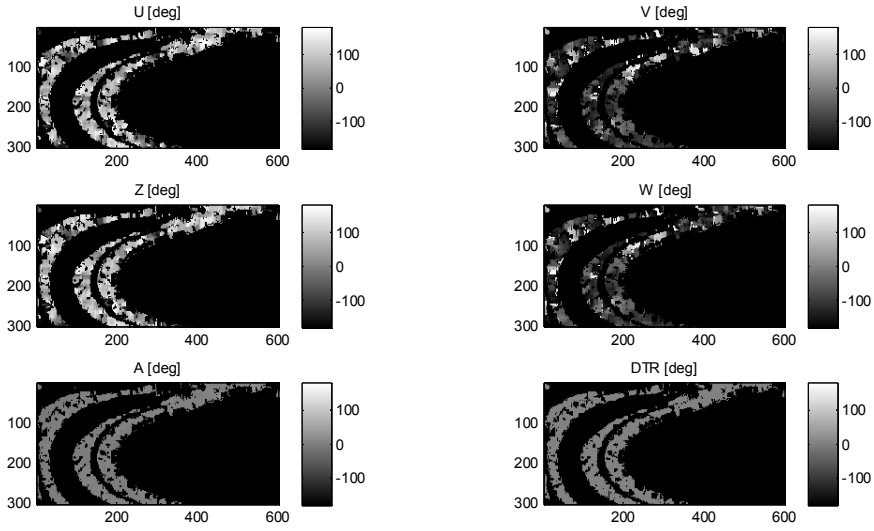


**Figure 5.14**. Results are shown using crosstalk calibration after before calibration method. The crosstalk ratios (i.e. $u$, $v$, $w$, and $z$) and the ratio of receive channel to transmit channel imbalance (i.e. $\alpha$) phase in degrees using the masked average covariance matrices are shown.

## 5.5 Resulting Imagery

The polarimetric crosstalk calibrated images are shown in Figures 5.15 and 5.16 for the method equations 3.43 and 3.11, respectively. The power of each is similar to the observed uncalibrated corresponding image. Comparison of crosstalk calibrated and uncalibrated show subtle difference in the cross-polarization channels as would be expected with stronger valued co-polarization scenarios.

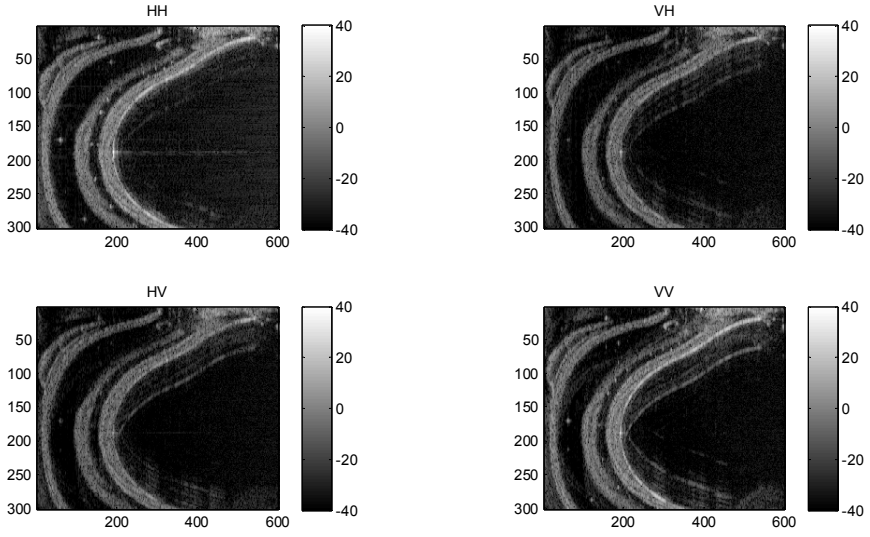


**Figure 5.15**. Blue Springs GBIR data are shown for the polarizations of HH (top left), VH (top right), HV (lower left), and VV (lower right) using crosstalk calibration after absolute calibration method. The images show the signal power in dB. The horizontal scale is slant range bins. The vertical scale is azimuth bins.

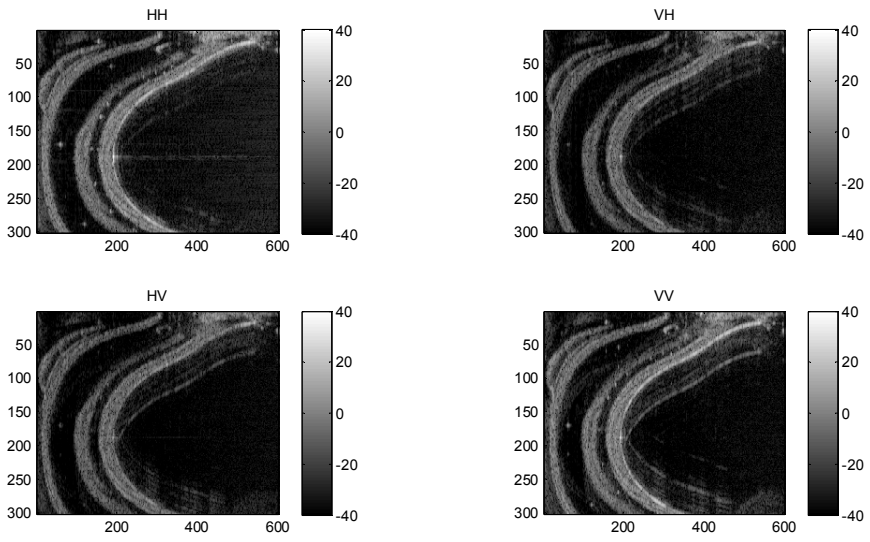


**Figure 5.16**. Blue Springs GBIR data are shown for the polarizations of HH (top left), VH (top right), HV (lower left), and VV (lower right) using crosstalk calibration before absolute calibration method. The images show the signal power in dB. The horizontal scale is slant range bins. The vertical scale is azimuth bins.

## 5.6. Summary

In closing, crosstalk calibration using global parameters produced about 9 dB improvement (i.e. From eqn 3.11 method, observed $v$ -16.4 dB reduced to $v$ calibrated -25.3 dB) for the Blue Springs Dam data set as shown in Table 5-1.

**Table 5-1**. Study global averages are shown for the crosstalk ratios and the ratio of receive channel to transmit channel imbalance.

| | ***A*** | | ***u*** | | ***V*** | | ***Z*** | | ***w*** | |
|---|---|---|---|---|---|---|---|---|---|---|
| **Scattering Matrix** | $\lvert\alpha\rvert$ | arg($\alpha$) | $10\log_{10}\lvert u\rvert^2$ | arg($u$) | $10\log_{10}\lvert v\rvert^2$ | arg($v$) | $10\log_{10}\lvert z\rvert^2$ | arg($z$) | $10\log_{10}\lvert w\rvert^2$ | arg($w$) |
| [$O$] Eqn. 3.5 | 1.11 | 16.8° | -25.1 dB | -64.0° | -16.4 dB | 77.4° | -26.5 dB | -57.8° | -19.9 dB | 58.7° |
| [$S$] Eqn. 3.43 | 1.00 | -0.3° | -27.3 dB | 86.7° | -24.8 dB | -93.3° | -26.9 dB | 86.5° | -24.9 dB | -92.8° |
| [$S'$] Eqn. 3.11 | 1.00 | -0.2° | -26.7 dB | 94.1° | -25.3 dB | -102.2° | -26.3 dB | 94.0° | -25.4 dB | -101.4° |

# 6. CONCLUSION & FUTURE WORK

## 6.1 Conclusion

An investigation into reducing crosstalk from Blue Springs Dam GBIR data was conducted using a standard model. Advanced polarimetric processing and techniques often rely on precise phase measurement. One benefit of crosstalk reduction is improvement in phase measurement. To achieve a successful estimation of the method parameters, data culling was performed to weed out low cross-polarization and high-correlation values from the processing flow. After data culling, average covariance matrices were formed for use in crosstalk parameter estimation. Analysis of crosstalk parameters demonstrated the values had small fluctuation over the unmasked locations. No apparent dominant range trends were observed in the parameters; therefore, estimations of the global values were found. Using the global estimates, calibration correction matrices were formed and applied to the data. The resulting crosstalk calibrated imagery showed a reduction in crosstalk of about 9 dB. Thus, the Blue Springs Dam polarimetric data were successful crosstalk calibrated.

## 6.2 Future Work

The results presented in this thesis may be valuable for future calibration efforts of the MU GBIR system. A number of avenues may be explored in future efforts. A few examples directions are listed below:

1. Absolute calibration using trihedral corner reflectors may be performed. At the time of this writing, a sufficient polarimetric GBIR data set with TCRs was unavailable.
2. Topography effects may be investigated. Although the crosstalk parameters in this study did not show strong range dependence, the crosstalk parameters did show some local variation. Local estimates of the crosstalk parameters due to topography (e.g. incident angle effects, local slope, etc.) and other effects may be performed.
3. Additional data culling masks may be explored for improving the estimation of the average covariance matrices.
4. Utilizing the crosstalk-calibrated fully-polarimetric data in various advanced processing polarimetric techniques. The study possibilities are vast in this area. A few examples of advance polarimetric processing opportunities are given below:
    a. Classification (e.g. land cover, change detection, etc.)
    b. Ground cover suppression (e.g. biomass, surface monitoring, etc.)
    c. Sub-pixel information retrieval (e.g. target detection, identification, etc.)
    d. Interferometry (e.g. DEMs, deformation mapping, subsidence, etc.)
    e. Polarimetric interferometry (e.g. improved interferometry, coherence optimization, , scatterer effects, etc.)

# BIBLIOGRAPHY


Advsolned. Website: http://www.advsolned.com/

Bonkowski, R., C. Lubitz, and C. Schensted (1953). Studies in radar cross-sections - vi. cross-sections of corner reflectors and other multiple scatterers at microwave frequencies. Technical report, University of Michigan Radiation Laboratory, October 1953. website: http://hdl.handle.net/2027.42/21139

Elachi, C., and Jakob van Zyl (2006). Introduction to the Physics and Techniques of Remote Sensing, John Wiley & Sons, Hoboken, New Jersey, 552 p.

Fore, A., B. Chapman, S. Hensley, T. Michel, and R. Muellerschoeny (2009). "UAVSAR Polarimetric Calibration," available: http://uavsar.jpl.nasa.gov/data/cal/UAV_cal.pdf

GAMMA Remote Sensing AG (2011). GAMMA Portable Radar Interferometer II (GPIR-II), GAMMA Remote Sensing AG, Switzerland. Gamma website: http://www.gamma-rs.ch/

Oppenheim, A. and R. Schafer (1989). Discrete-Time Signal Processing, Prentice Hall, Englewood Cliffs, New Jersey, 879 p.

Papathanassiou K., and M. Zink (1998). "Polarimetric Calibration of the Airborne Experimental SAR System of DLR," *Proceedings of European SAR Conference*, EUSAR 1998, Friedrichshafen, Germany, pp. 259-262.

Quegan, S. (1994), "A unified algorithm for phase and cross-talk calibration of polarimetric data-theory and observations", *IEEE Transactions on Geoscience and Remote Sensing*, Vol. 32, No. 1, pp. 89-99.

Radar Tutorial. Website: http://www.radartutorial.eu/

Richards, M (2005). Fundamentals of Radar Signal Processing, McGraw-Hill, New York, 513 p.

Skolnik, M. (1990). Radar Handbook. McGraw Hill, Boston, Massachusetts, 1200 p.

Skolnik, M. (2008). Radar Handbook, McGraw-Hill Company, New York, 1328 p.

Tamatsu, Y., H. Hazumi, and H. Nakatani (1997), "FMCW RADAR SYSTEM", US Patent NO. 5,619,208, April 1997.

Ulaby, F., R. K. Moore, and A. K. Fung (1982). Microwave Remote Sensing Active and Passive Volume II, Artech House, Norwood, MA, 1064 p.

Ulaby, F. (2007). Fundamentals of Applied Electromagnetics. Pearson Prentice Hall, Upper Saddle River, NJ, 464 p.

van Zyl, J. and Y. Kim (2011). Synthetic Aperture Radar Polarimetry. John Wiley & Sons, Inc., Hoboken, New Jersey, 288 p.

Werner, C., T. S., A. Wiesmann, and U. Wegmüller (2009), "A Ground-based Real Aperture Radar Instrument for Differential Interferometry", *IEEE Radar Conference 2009*, 4-8 May 2009.

# APPENDIX A:

Average crosstalk and imbalance parameters are plotted by range bin. Blue refers to [*O*]. Green refers to [*S*]. Red refers to [*S'*]. Global averages are used in chapter 5.